

ELECTROPHYSIOLOGICAL ANALYSIS OF OPTICALLY ACTIVE STEM CELL DERIVED MOUSE NEURAL NETWORKS

By

NICHOLAS JAMES SOLOMOTIS

(Under Direction of Steven L. Stice)

ABSTRACT

Understanding neural networks and their characteristics leads to the establishment potential research models or targets for treatments of neuromuscular and other neurodegenerative diseases. Multielectrode array (MEA) technology and optogenetics, the integration of light-sensing ion gated channels, gives researchers the ability record communication between cells and allow for the analysis of emergent behavior and characteristics of developing neural networks. This study uses HBG3 Chr2 mESC's with directed differentiation toward motor neurons to form mixed population neural networks on the MEA. Pharmacological treatments demonstrated functional inhibitory and excitatory responses for both glutamate and GABA receptors. After repeated light exposure, the effective integration of the Chr2 protein was seen in raster-plot analysis. Proving that the activity of

these networks can be controlled both pharmacologically and optically will lead to a higher degree of network manipulation and allow for the establishment of advanced multipurpose models for further investigation of neurological connectivity, functions, and diseases.

INDEX WORDS: MEA, Optogenetics, ChR2, NMDA, AP5, AMPA, GABA, Bicuculline, Glycine

ELECTROPHYSIOLOGICAL ANALYSIS OF OPTICALLY ACTIVE
STEM CELL DERIVED MOUSE NEURAL NETWORKS

by

NICHOLAS JAMES SOLOMOTIS

B.S., University of Maryland, 2013

A Thesis Submitted to the Graduate Faculty of The University of Georgia in

Partial Fulfillment of the Requirements for the Degree

MASTERS OF SCIENCE

ATHENS, GEORGIA

2015

© 2015

NICHOLAS JAMES SOLOMOTIS

All Rights Reserved

ELECTROPHYSIOLOGICAL ANALYSIS OF OPTICALLY ACTIVE
STEM CELL DERIVED MOUSE NEURAL NETWORKS

by

NICHOLAS JAMES SOLOMOTIS

Major Professor: Steven L Stice

Committee: Hongxiang Liu
Lohitash Karumbaiah

Electronic Version Approved:

Julie Coffield
Interim Dean of the Graduate School
The University of Georgia
May 2015

ACKNOWLEDGEMENTS

I'd like to thank my parents for their unconditional support,

Even though my dad who initially thought I sold short.

Appreciation for my friends and colleagues that listened to my incessant

whining,

With assurance that at the end there existed a silver lining.

Although a wake of destruction follows you that can be measured in

substantial dollars,

Nubi, your unconditional devotion almost made up for my lack of lady

callers.

To my major professor Dr. Steven L Stice, your patience did not go

unnoticed.

And through all my pestering, bitching and moaning,

You helped me despite my neurotic droning.

With repeated feelings of apprehension and trepidation,

I could not have finished without loads of medication.

You all have made my experience something I will treasure,

I will never forget Georgia and it's southern pleasure.

TABLE OF CONTENTS

	Page
ACKNOWLEDGEMENTS	iv
LIST OF TABLES	vii
LIST OF FIGURES	viii
CHAPTER	
1. MOTOR CONTROL	1
2. ELECTROPHYSIOLOGY OF NEURONS AND NEURAL NETWORKS	6
3. NEURAL PHARMACOLOGY	17
4. EMBRYONIC STEM CELLS TO NEURAL NETWORKS	25
5. OPTOGENETICS: LIGHTING THE ROAD TO THE FUTURE	29
6. ELECTROPHYSIOLOGICAL ANALYSIS OF OPTICALLY ACTIVE MOUSE EMBRYONIC STEM CELL DERIVED NEURAL NETWORKS	
Introduction	34
Experimental Procedures	37
Results.....	43
Discussion	48
Acknowledgements.....	52

7. CONCLUDING REMARKS AND FUTURE DIRECTIONS	81
REFERENCES	87

LIST OF TABLES

	Page
Table 3.1: Neurotransmitter Summary	24
Table 6.1: Developmental Changes of HBG3 ChR2 Neural Networks	57
Table 6.2: NMDA Results	58
Table 6.3: NMDA Results	61
Table 6.4: AP5 Results.....	64
Table 6.5: AMPA Results	67
Table 6.6: GABA Results	70
Table 6.7: Bicuculline Results	73
Table 6.8: Glycine Results	76
Table 6.9: Optogenetic Results.....	79

LIST OF FIGURES

	Page
Figure 1.1: Motor Pathway.....	3
Figure 1.2: Spinal Cord Development.....	4
Figure 2.1: Microelectrode Array Plate Well.....	12
Figure 4.1: Embryonic Stem Cell Development.....	26
Figure 5.1: Channel Rhodopsin-2 Receptor	30
Figure 6.1: Experimental Set-Up.....	53
Figure 6.2: Developmental Changes of HBG3 ChR2 Neural Networks.....	55
Figure 6.3: NMDA Raster Plots	59
Figure 6.4: AP5 Raster Plots.....	62
Figure 6.5: AMPA Raster Plots.....	65
Figure 6.6: GABA Raster Plots	68
Figure 6.7: Bicuculline Raster Plots	71
Figure 6.8: Glycine Raster Plots	74
Figure 6.9: Optogenetic Raster Plots.....	77

1. MOTOR CONTROL

“Cogito ergo sum” translated to “I think, therefore I am” is a famous quote by René Descartes meaning that our existence is proven by the fact that we are conscious of it. This famous quote has been altered on several occasions, but one of the more relevant alterations is “I move, therefore I am.”

Everyday we perform actions. Whether it's walking, driving, typing, etc., these actions all require controlled movement [1]. This control of your actions or movements confirms that we are in fact a living being [2]. How we control these actions have been studied for over a century, but even today we are still making new discoveries [3].

All voluntary movements start with the Central Nervous System (CNS), which includes the brain/brainstem, the spinal cord, and the cortex [4]. A motor command is generated in the motor cortex in the CNS and sent to the motor neurons, which signal the muscle to cause a muscle contraction [3]. This led to the discovery of what is commonly referred to as motor units. Motor units are mosaic combinations of nerves and muscles that include a

synaptic junction in the ventral root of the spinal cord, a motor neuron, and a motor end plate in the muscle fibers [5]. A motor unit can control as many as 2000 muscle fibers or as little as three depending on the muscle [5].

Finger and face muscles have small shorter fibers, while the muscles of the legs have many long fibers in their respective motor units. Depending on the muscle size, multiple motor units can be recruited. The motor pathway includes both inhibitory and excitatory synaptic junctions that work together to control the final junction on the spinal cord to control the motor units [5].

The motor neurons in the spinal cord are commonly referred as the final common pathway for all motor output including interneurons that integrate sensory feedback from the skin, muscles and joints [4].

More recent studies have come up with the concept of the central pattern generator (CPG). First described in invertebrates, the CPG is a neuronal network capable of creating organized patterns of motor activity without the need of sensory inputs [6]. The locomotor CPG, located in the spinal cord, has its outputs determined by inputs from the brainstem and descending parts [6]. The locomotor CPG is made of a dispersed network of motor neurons and interneurons that generate organized motor rhythms when appropriately stimulated. Motor pools are the main feature of this organized

activity. A motor pool is composed of groups of motor neurons in discrete operational units. Each motor pool stimulates a single muscle [6]. However, none of this can happen without the initial development of motor neurons.

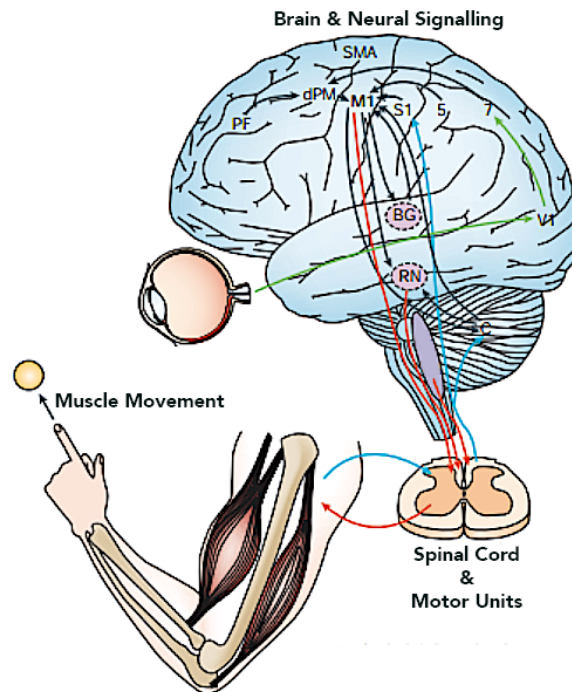


Figure 1.1: Motor Pathway

Movement starts in the brain. A signal for motor behavior is created in the brain and sent to the spinal cord and motor neurons. The signal is then sent from the motor neurons to the muscles. The muscles contract and movement is achieved. (Adapted from [4])

Motor Neuron Development

The spinal cord is one of the major components of the CNS. Within the spinal cord there exists a large diversity of neuronal cell sub-types, many of which are used in motor control [7]. The fate of these cells is largely determined by two main signaling systems acting synchronously, one along

the rostrocaudal axis and the other along the dorsoventral axis. The spinal cord can be further divided into multiple domains. The floor plate is the most ventral of the domains followed by the V3 domain, then pMN (progenitor motor neuron) domain, then V2, V1, and V0 domains. V0 through V3 are identified as different types of ventral interneurons [7]. The divergence of neuronal subtypes is largely due to a gradient of Sonic hedgehog (Shh), a protein secreted by the notochord. Ventral domains require higher concentrations of Shh (Fig. 1.2). Retinoid signaling also plays large role in both spinal cord and neuronal subtype identity [7] through caudal induction [8].

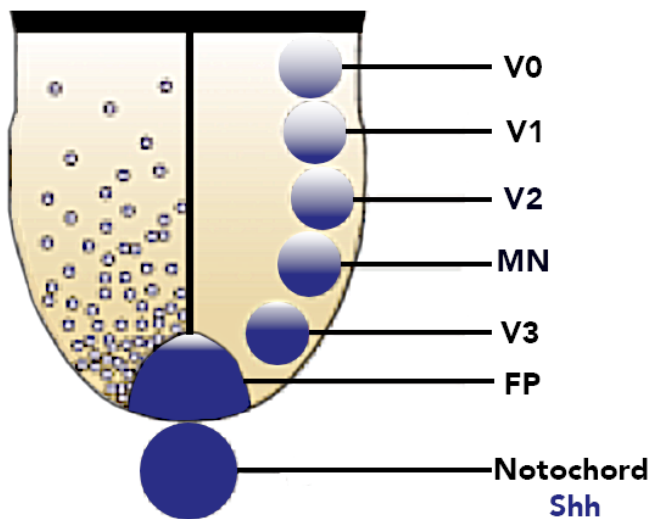


Figure 1.2: Spinal Cord Development

Representative diagram of the Sonic hedgehog's (Shh) morphogenic expression in the developing neural tube. Shh is secreted by the notochord. Circles with more blue indicate a higher concentration of Shh exposure. With such close proximity to the notochord, the floor plate is the first to develop which also starts secreting Shh. Higher concentrations of Shh will

induce motor neuron and ventral interneuron 3 differentiation, while lowers concentrations will induce differentiation of ventral interneurons 0-2. (Adapted from [7])

Motor neuron differentiation requires both increased Shh and retinoid signaling [8]. The key neuronal subtype for motor control, motor neurons are the last signaling step before the muscles and, as previously mentioned, are known as the final common pathway for all motor output [4]. To complete these complex tasks, motor neurons, as well as all neuronal subtypes, possess distinct characteristics resulting in unique signaling mechanisms and traits.

2. ELECTROPHYSIOLOGY OF NEURONS AND NEURAL NETWORKS

The main distinction between neurons and other cell types is that neurons are polarized, having specific morphological regions for specific functions, dendrites that receive signals and an axon that transmits a new signal. The interactions of the axons and dendrites allow neurons to send and receive multiple types of signals [9]. Feedforward excitation is one neuron sending information to its neighbor. This is common in long chains in the nervous system. There's also feedforward inhibition. This is when an inhibitory interneuron is excited and then inhibits the next receiving cell, which controls and limits the excitation in a neural circuit. Feedforward excitation and inhibition are well understood and contribute to motor reflex performance, commonly observed at the doctor's office with the knee jerk reflex test. The hammer to the knee followed by the extension of the leg demonstrates the fidelity of that specific sensory motor pathway in the spinal cord [9].

Convergence signals are when one neuron receives input from multiple other neurons in a network, while divergence is when one neuron sends information to multiple neurons in a network. Convergence and divergent signals are particularly relevant in the motor pathway. A single sensory neuron has to be able to send signals to multiple motor neurons simultaneously. This allows collective muscle fiber contraction from numerous motor neurons [9]. Proper function of these network motifs make it easy to see how malfunctions, such as in a case where sensory neurons ability to signal multiple motor neurons is restricted, could cause flexibility or strength complications.

Lateral inhibition is similar to feedforward inhibition except that the inhibitory neuron is inhibiting cells in close proximity in a network. Our optic/visual information processing pathway is one such example that implicates lateral inhibition. The ability for the photoreceptors to inhibit the second order neurons helps define the edges and borders of what one is viewing [9]. Blurred edges could pose problems in simple daily functions such as reading, where distinguishing letters might prove to be more difficult.

Feedback inhibition occurs when either an excitatory neuron excites another excitatory neuron that excites an inhibitory neuron which then inhibits the initial excitatory neuron or when successive inhibitory neurons inhibit each other in a closed chain. Feedback inhibition is a critical motif with predicted associations with multiple functions, including circadian rhythms and motor behavior. Having both excitatory and inhibitory neurons in a closed chain grants the ability for the generation of multiple patterns with a minimal number of neurons making this process highly energy efficient. This can be easily seen in the gaits of quadrupeds. Depending on their speed, their legs move in different arrangements whether their alternating in a trot or moving together in a bound [9].

Finally, feedback excitation just replaces the inhibitory neurons from feedback inhibition with excitatory neurons creating a loop of excitatory neurons. Complex circuits of feedback excitation in the hippocampus contribute to the ability to store and recall information, a necessary function to survive. The consistent excitation loops progressively strengthen these connections [9].

Among the types of signaling, polarization also gives neurons specific electrical properties; endogenous bursting, postinhibitory rebound, spike frequency adaption, and plateau potentials [6]. Endogenous bursting is demonstrated in some isolated neurons through firing in spontaneous bursts or in response to a neuromodulator [6]. Postinhibitory rebound occurs when a neuron is hyperpolarized. This causes the membrane potential to reverse resulting in a single action potential or train of action potentials that contributes to rhythm generation [6]. Spike Frequency adaption occurs when neurons will fire initially, but then adjust to stop firing if needed [6]. Plateau potentials happen when short excitatory inputs can cause extended depolarized states while short inhibition cause hyperpolarized states. These properties are particularly important in the interactions between interneurons and motor. The relationship between spinal interneurons and motor neurons is still poorly understood. Identification of these properties will hopefully lead to a deeper understanding on interneuron motor regulation and how they all work together for proper locomotion [6].

Two electrophysiological properties, not unique to, but commonly seen in motor neurons are spike frequency adaption (SFA) and rebound action potentials (RAP). SFA is an increase in interspike interval (ISI), the time

between spikes, as a response to a constant depolarizing current possibly aiding in the development of prolonged muscle contractions for smooth muscle movement. RAP, a specific bursting discharge pattern, is thought to be involved with the generation of rhythmic bursting and firing patterns in order to perform proficient muscle contractions [10].

With all these different properties and signaling, neural plasticity becomes an essential quality of neural networks. Neural networks have to interpret constant streams of ever changing activity from visual, auditory, and sensory signals. This interpretation is very important for supporting a base for learning and long-term memory storage that involve a plethora of changes in membrane excitability and synaptic transmission [11]. Neural plasticity refers to a network's ability to make modifications to its circuitry in response to external or internal stimuli. These adjustments prepare the network for subsequent feelings, thoughts, and behaviors [12, 13]. Neural plasticity is even relevant when dealing with physical trauma. If a region of the cortical network is damaged, nearby cortical neurons will cover for the functions normally performed by the injured area [12]. Neural plasticity guarantees stability and signal-dependent functionality of the networks [11].

A lot of disorders and diseases stem from or involve deficiencies or malfunctions of these different properties and circuits. Scientists need a way to monitor and manipulate them on network wide scale.

Recording and Stimulation of Cell Electrophysiology

Multi-/Microelectrode Arrays (MEA) provide the means for successfully testing and manipulating the functionality of neural networks in vitro. MEA's are made of two main pieces. Physical electrode arrays, made from either tin, gold, or platinum, interact with the plated tissue or cell cultures and receive the signals which are then interpreted through integrated electronics [14]. The main attraction to these machines is the ability to view, record, and stimulate the electrical activity of electrically active cell types, such as neurons and cardiomyocytes, for extended periods of time [15], unlike patch clamps which only are able to record the activity from a single cell at a time [16].

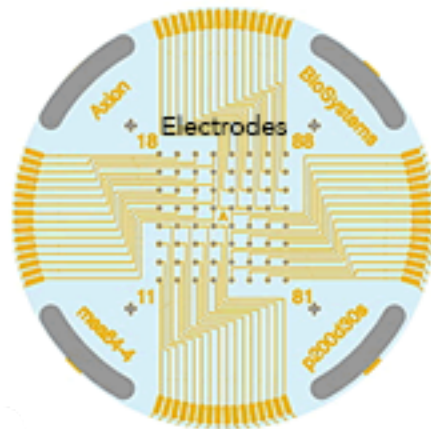


Figure 2.1: Microelectrode Array Plate Well

Representative diagram of a standard MEA plate well from Axion Biosystems. This particular example features 64 electrodes that possess the ability to record electrical data from single cells to entire networks. (Adapted from [14])

The first MEA was developed in 1972 with limited capabilities, only being able to record activity from cardiac cells [17]. Ten years later (1982), the first electrical potentials of mammalian CNS neurons, dissociated from spinal cord tissue, cultured on the electrode surface were recorded [15]. The ability to record neural network potentials, an incredibly important advancement, demonstrated the potential of the MEA systems. Fast forward to today, labs have successfully recorded electrical activity from ex vivo (brain slices), in vitro neural networks (primary neural networks), and even embryonic stem cell derived neural networks on the MEA systems [18].

Analysis of Neural Activity

The programs that pair with the MEA systems and are able to record neural activity, such as Axion's AxIS (Axion Integrated Studio) program, generate an abundance of data. Software such as Neuroexplorer [19], MATLAB [20], and Axion's Neural Metrics program is used to aid with the organization and interpretation of the data and does a lot of the hard work for scientists today in determining burst and synchrony parameters. The programs use established algorithms that are used to convert the raw data to the desired neural metrics: be it inter-spike-intervals, burst frequencies, cross-correlations for synchrony, inter-burst-intervals, etc. However, there is a lot of debate as to what the best algorithm is to determine parameters like bursting, so some groups still choose to analyze their data the hard way and use their own formulated algorithms [21-23]. In the end, the algorithms used for the programs are up to the developers and what they consider to be the most valid.

Some of the more advanced programs will even create plots and graphs with the selected data set. Raster plots are often used to as a visual representation of network activity over a set period of time. Generally, a raster plot consists of each row displaying the activity from an individual

electrode with each black line or “tick” indicating a single spike. These plots provide a basic idea of firing rates, bursting, and synchrony of network activity without the use of actual numbers [24]. Axion’s Neural Metrics Tool even accompanies rate histograms with their raster plots to provide a more informative visualization of network firing rates.

Synchronous activity is a characteristic indicative of mature neural networks. Synchrony is the measure of interaction between activity of neurons in a population, or in the case of MEA’s, a correlation between electrode activity in a well. Synchrony within extensive neural populations contributes a crucial role in the processing of sensory and cognitive information. To measure network synchrony, researches often employ a cross-correlation analysis. In layman terms, a cross-correlation algorithm measures the time or distance between the spiking at multiple points. Synchrony windows, designated times between spikes to consider the activity synchronous, are usually defined by the researcher. Highly synchronous activity is modeled by a large peak at 0 seconds on a cross-correlogram. This means that the majority of the activity between the electrodes falls within the set window designating firing at the same time in a consistent manner [25].

Due to considerable amounts of variation between recorded electrodes, filters are specified to refine the data for analysis. These filters are set to dampen the influence from ambient noise and outliers. Previous studies have established specified parameters for their data analysis. Electrodes with high ambient noise ($>10\mu\text{V}$) could contribute false signals. These electrodes are deemed "noisy electrodes" and are excluded from the data analysis [19, 26, 27]. Studies also eliminate electrodes that aren't considered active or designated as silent. An "active electrode" is one that records a specified firing rate. Previous studies have set an "active electrode" to be one that records at least 5 spikes per min [19, 26, 27]. With multi-well MEA plates where wells are the specified "n" or unit of measurement, a filter is set to determine an "active well." These are wells that have a designated number of "active electrodes". Electrodes and wells that do not meet these requirements are excluded from the data analysis [19, 26, 27].

Unfortunately even with the filters set to reduce noise and variability contribution to data, variation between electrodes still manages to weasel into the data. Weighted averages of well activity based on the number of "active electrodes" are used as a more suitable method to represent the neural metric variables [26, 27]. Weighted values provide a more accurate

representation of the results. Wells with a higher number of active electrodes contribute a greater effect on the final weighted average reducing the influence of possible outliers.

The MEA technology has been updated with the ability to interpret spike, burst, and waveform patterns for extensive and compound analyses of tissue and cell culture electrophysiology. With the creation of multi-well MEA systems, MEA's have proven to be a great asset for pharmacological studies and recording the electrophysiological responses of pharmacological treatments on neural networks. As a result, labs are able to determine the functionality of neural receptors in vitro neural networks to use as a model for their in vivo counterparts [24].

3. NEURAL PHARMACOLOGY

When neurons send messages to each other, they release small molecules known as neurotransmitters. These pharmacological reagents can be inhibitory, excitatory, or both, and it is this balance and control that allows us to function on a daily basis. Neurotransmitters are synthesized and released from the presynaptic terminal of neuron, which is then received, by the postsynaptic terminal of another neuron. Neurotransmitters range from specific amino acids and their derivatives, biogenic amines, peptides, gases, and many other small molecules [28]. The type of signal produced depends on the neurotransmitter and can regulate a diverse variety of functions ranging from as large scale as movement to molecular gene expression. Neurotransmitter regulation is a very complex process and disruptions of the balance can lead to death, paralysis, mood or behavior changes, and diseases like Parkinson's [28].

Glutamate: “I’m So Excited and I Just Can’t Hide It”

Glutamate or L-glutamic acid is the most common excitatory neurotransmitter, and neurons that release glutamate are said to be glutamatergic [13]. Research has proven that not only is glutamate important for excitatory signals, but plays important roles in neuronal migration, neural differentiation, brain development, axon genesis, neuroplasticity, and neuronal survival [13].

There are two main glutamate receptors: ionotropic (ligand-gated) and metabotropic (G protein-coupled) [29]. The ionotropic receptors (iGluRs) can be further split into either ion-gated, α -amino-3-hydroxy-5-methyl-4-isoxazole propionic acid (AMPA) and kainate (KA) receptors, (AMPA/KARs) and voltage-dependent (via Mg^{2+}), N-methyl-D-aspartic-acid (NMDA) receptors (NMDARs) [13]. iGluRs are all gated cation channels were classified based on their pharmacological characterization, agonist specificity, and genetic sequence [30].

AMPA receptors are most permeable to Na^+ and are large contributors to excitatory neurotransmission and synaptic plasticity; abnormalities with AMPARs are linked to a variety of neurodegenerative illnesses. AMPARs have a large

involvement in seizure-induced neuronal injury and seizure activity and expression; thus it has been linked as a major contributor to epilepsy [31].

The main characteristic that separates NMDARs is the involvement of co-agonists, such as glycine or D-serine needed for activation. NMDAR's have a high permeability to Ca^{2+} and NMDA receptor-mediated signaling plays substantial roles in neural development, learning, memory, plasticity, and high cognitive functions. Because of NMDAR's large part in the formation and functionality of synapses and temporal integration of neural network activity, mutations or dysfunctions are associated with neurodevelopmental disorders [32].

AP5 also referred to as APV (2-amino-5-phosphonovalerate), a competitive NMDA antagonist as well as AMPAR's respective antagonists, such as DNQX (6,7-dinitroquinoxaline-2,3-dione) and CNQX (6-cyano-7-nitroquinoxaline-2,3-dione), are commonly used pharmacological treatments to study the functionality of glutamate receptors in neural networks [33, 34].

GABA: “The Inhibinator”

Although excitatory early in development [35, 36], gamma-aminobutyric acid (GABA) is the premiere inhibitory neurotransmitter in the CNS of developed vertebrate [13, 35]. Neurons that produce GABA are referred to as GABAergic. As an inhibitory neurotransmitter, activation of their receptors causes a hyperpolarization or decrease of the membrane potential due to an inward flux of chloride ions (Cl^-) [37]. Research has shown that GABA stimulates dendritic development in both late embryonic stages and adult neurogenesis [36].

There are 3 types of GABA receptors (GABARs); the ionotropic GABA_A and GABA_C and the metabotropic GABA_B . GABA_A receptors (GABA_ARs) are straight Cl^- -gated channels sensitive to bicuculline, a GABA_A competitive inhibitor. GABA_B receptors (GABA_BRs) couple to Ca^{2+} and K^+ channels with the assistance of G proteins and messenger systems sensitive to its competitive inhibitor baclofen. GABA_C receptors (GABA_CRs) are often referred to as a subset of GABA_ARs , but are inhibited by neither bicuculline nor baclofen. These three receptors are genetically and structurally unique as well as having distinct cellular localization [35].

GABA_ARs are the most studied receptor because it is the site of benzodiazepines and barbiturates, drugs commonly used as depressants. GABA_AR is also the target of general anesthetics, alcohol, and neurosteroids, and many CNS excitants [13] as well as a key player in the regulation of pain in the spinal cord. Malfunctioning of GABA_AR results in persistent pain [38].

GABA treatments on the MEA result in a reduction of activity. The addition of bicuculline, has shown to induce synchronous bursting and rescue activity lost when previously treated with GABA proving the functionality and conservation of GABA_A receptors in mouse, rat, and human neural networks [33, 34, 39].

Glycine: "Goes Both Ways"

Glycine is the other main inhibitory neurotransmitter of the CNS, but is more prominent in the spinal cord, specifically the dorsal horn [40] and activates Cl⁻-gated glycine receptors (GlyRs) [13]; however, glycine can also act as an excitatory neurotransmitter through its role as a co-agonist of NMDA glutamate receptors [32].

Similar to GABA_ARs, GlyR's is also association with neuropathic pain and inflammatory processes. As a result, drugs that inhibit glycine transporters (GlyTs), or amplify inhibitory neurotransmission, are often used for nociceptive and inflammatory treatments [40]. GlyT1 and GlyT2 are the two types of glycine transporters responsible for the regulation of GlyR and NMDAR activity. GlyT1 are expressed in a subpopulation of glutamatergic neurons as well as both inhibitory and excitatory synapses of astrocytes, while Gly T2 is strictly located at the presynaptic terminals of inhibitory glycinergic neurons [41].

Acetylcholine: To Move or Not to Move

The iconic neurotransmitter involved in motor control is acetylcholine (ACh). Cells that produce and release acetylcholine are cholinergic. Cholinergic neurons are quite prominent in the CNS and PNS. Cells contain one of two types of acetylcholine receptors; the metabotropic muscarinic receptors or the ionotropic nicotinic receptors [13].

Acetylcholine is the neural transmitter most commonly released by the motor neurons. and is sent to the muscles inducing contraction and thus movement. Besides skeletal muscle, research has shown that acetylcholine

contributes to smooth muscle contraction and possesses key roles in inflammatory and remodeling responses [42] as well as having involvement in arousal, sleep, motivation, rewards and other cognitive processes [13].

A sharpened understanding of these receptors improves techniques to control the electrophysiological properties such as changes in membrane potentials or formation of action potentials and links between pharmacological receptors and neurological/neurodegenerative diseases provide research targets for potential treatments for these conditions:

AMPA_Rs as a target for epilepsy treatment [31], GABA_A_Rs or Gly_Rs for spinal pain [38], NMDA_Rs for treatments of stroke, pain, schizophrenia, and other neurological and psychiatric disorders [43], and acetylcholine and other nicotinic receptors as a treatment target for Alzheimer's or motor function diseases [44].

Neural research requires the acquisition of large quantity of cells. A cell type that could provide an infinite access to neural subtypes as well as provide information on neural development would prove to be quite useful.

Embryonic stem cells provide this advantage.

Table 3.1: Neurotransmitter Summary

Neurotransmitter	Receptors	Excitatory (E) / Inhibitory (I)	Most Permeable Ion	Functions/Associations	Ref
Glutamate	NMDA AMPA	E E	Ca ²⁺ Na ⁺	learning, memory, seizure	26, 27
GABA	GABA _{A-C}	I	Cl ⁻	pain, alcohol, neurosteroids	13, 33
Glycine	NMDA Glycine	E I	Ca ²⁺ Cl ⁻	pain, inflammation, (see NMDA)	35
Acetylcholine	Nicotinic Muscarinic	E E	Na ⁺ /Ca ²⁺ Na ⁺ /Ca ²⁺	movement, inflammatory response, arousal, sleep	37, 13

4. EMBRYONIC STEM CELLS TO NEURAL NETWORKS

The applications of stem cell technology are near limitless. Embryonic stem cells (ESC's) are both immortal and pluripotent, continuously dividing while possessing the capability to differentiate into any cell type from all 3 germ layers, including skeletal, cardiac, pancreatic, hematopoietic, epithelial, and neural [45, 46]. ESC's are isolated during the blastocyst stage of embryonic development from the inner cell mass and maintain the ability to keep their pluripotency, self-renewal, and infinite proliferation potential in vitro [46, 47]. Specific advantages, especially with neuronal cultures, include the uses for cell therapy, developmental studies, and toxicology screening for drugs and other applications [48].

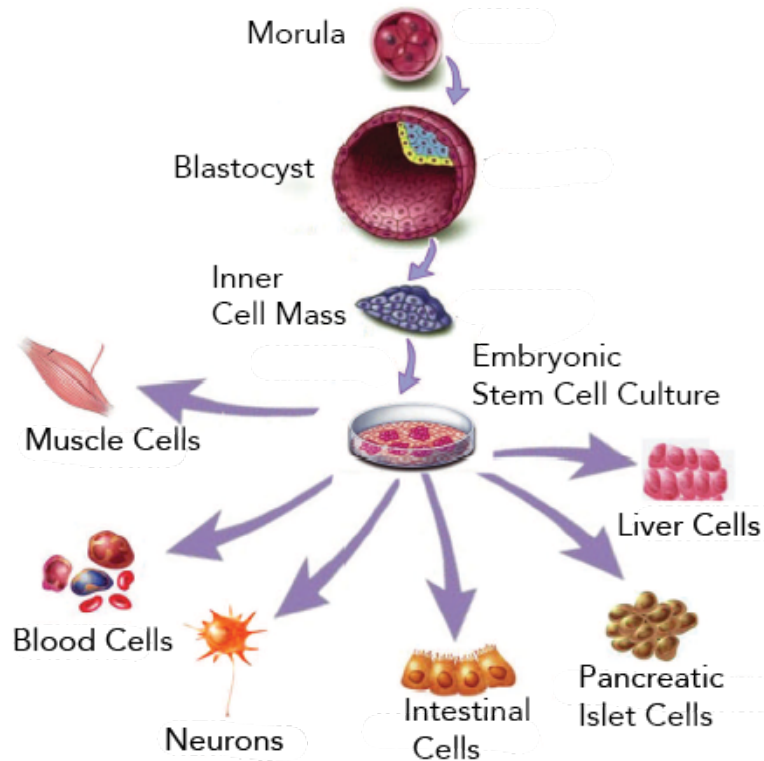


Figure 4.1: Embryonic Stem Cell Development

Embryonic stem cells are isolated from embryos during the blastocyst stage of development. These cells expand infinitely while sustaining the ability to differentiate into a variety of cell lineages including muscle cells, blood cells, neurons, intestinal cells, pancreatic islet cells, and liver cells to name a few. (Adapted from [46])

Embryonic stem cells are able to differentiate into a plethora of neural subtypes including cortical neurons, dorsal interneurons, glial cells, and even spinal motor neurons [48]. Isolating motor neurons from mammals is not the easiest task, especially in humans, so the ability to differentiate stem cells into motor neurons is a beneficial.

Differentiation into motor neurons is obtained through two main gradients, Shh and retinoid signaling [8]. In order to differentiate ES cells into motor neurons, these gradients have to be mimicked. ES cells are formed into embryoid bodies (EB's), large usually spherical colonies of cells. The EB's are then exposed to both retinoic acid (RA) and Shh or purmorphamine, a Shh agonist [8, 45]. The retinoic acid caudalizes the fate of the cells towards spinal progenitors and the purmorphamine ventralizes the cells' fate to progenitor motor neurons, the pMN domain [48].

Stem cell derived motor neurons have demonstrated similar electrical properties, such as SFA and RAP to primary motor neuron cultures [10] and have been successfully transplanted and innervated into denervated sciatic nerves of mice [49]. The advantages of stem cell derived motor neurons also includes improved investigation of motor neuron diseases like amyotrophic lateral sclerosis (ALS) or spinal muscular atrophy (SMA) [47] as well as the possible inclusion for the use of biological robots and organoids [50].

With MEA technology, we can more effectively investigate the changes in electrophysiology during the development and maturation of neural networks. In 2007, mouse embryonic stem cells (mESC's) differentiated

towards GABAergic neurons provided results similar to both hippocampal and cortical primary cultures on an MEA [20]. The mESC-derived neurons showed spontaneous activity, a characteristic indicative of primary cultures as well as the appearance of spike bursts, spike trains and synchronous firing, providing evidence of a maturing network. When electrically stimulated through the MEA, propagation of the evoked activity was seen across the network similar to what had been previously seen with both cortical and hippocampal primary cultures [20].

To further confirm mESC-derived neural networks as a functional substitute, mESC-derived neural networks on the MEA were exposed to pharmacological treatments such as GABA, NMDA, and their respective antagonists (bicuculline and APV) as well as the neurotoxin tetrodotoxin (TTX). The results again showed similar electrical responses to primary neuronal cultures further providing evidence that ES-derived neural networks can functionally mimic the physiological network characteristics and be used as a useful tool for future electrophysiological studies [33]. Similar results have also been confirmed with human embryonic stem cell (hESC)-derived neural networks [34].

5. OPTOGENETICS: LIGHTING THE ROAD TO THE FUTURE

Recent advancements in genetic engineering have created a new method to stimulate cells. Cells can be manipulated to allow optical stimulation by different wavelengths of light. Inserting the genes for light sensing proteins into neurons or other cell types allow for cellular functions or characteristics, such as membrane potential and bursting patterns, to be controlled by light [51].

Channelrhodopsin-1 (ChR1) and channelrhodopsin-2 (ChR2) are the two most widely proteins whose genes are inserted for optical control. First classified in single-cell green algae, *Chlamydomonas reinhardtii*, many rhodopsin homologs to have been identified in other species and the numbers continue to grow[51]. As cell membrane proteins, rhodopsins function as ion channels that respond to light, consisting of about 300 amino acids that make up seven transmembrane helices. Light absorption results in a conformational change of the protein, allowing in the case of channel rhodopsin, cations, such as Na^+ , K^+ , Ca^{2+} , and H^+ to permeate the cell

inducing a photocurrent and thus a change in membrane potential that spans across all cells containing the protein (Fig. 5.1) [51].

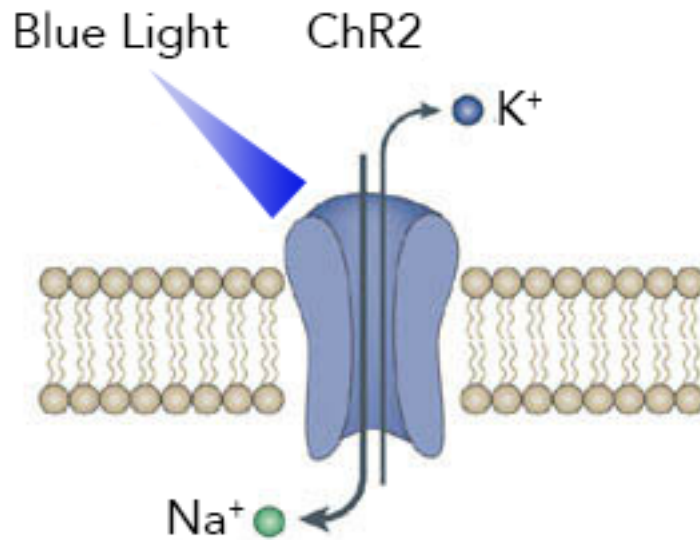


Figure 5.1: Channel Rhodopsin-2 Receptor

Representative digram of channel rhodopsin-2 receptor. Exposure to blue light causes the channel to open and allows the permeation of positively charged ions such as Na⁺ and K⁺. (Adapted from [52])

ChR2, the protein used in this experiment, is one of the more commonly used rhodopsin. ChR2 activates when exposed to blue light with peak absorption between 460-470 nm. When expressed in neurons, blue light exposure causes an influx of sodium and calcium ions, which generates a membrane depolarization resulting in an action potential. There are also rhodopsin proteins that hyperpolarize membrane potentials when stimulated. Halorhodopsin (NpHR) is a Cl⁻-transporting rhodopsin and archaerhodopsin (Arch) is an H⁺-transporting rhodopsin. NpHR pumps Cl⁻

ions into the cell, while Arch does this by pumping H⁺ ions out of the cell [53].

VGAT-ChR2 transgenic mice (ChR2 integrated into GABAergic neurons), demonstrated that by shining blue light on specific sections of the spinal cord or brain, they were able to inhibit hind-limb movement. Hind limb function instantly recovered after exposure. The blue light induced positive action potentials in inhibitory interneurons causing a downstream inhibition of hind-limb movement [54]. This is just one example that exemplifies the precise manipulation of neural circuits through optogenetics.

Optogenetics have also been used to help integrate transplanted neurons [49]. Embryonic stem-cell derived motor neurons have been shown to integrate with denervated muscle in mice, but not well with the descending signals from the CNS. This means the activity requires regulation by a separate control system. One option is to electrically stimulate them, but that stimulates the native neurons as well, not just the transplanted. This is where optogenetics shines. By transplanting ChR2 ESC derived motor neurons into a denervated peripheral nerve, blue light can successfully

stimulate strictly the engrafted motor neurons, leaving the native signals alone, and helping integrate the recruitment of motor units [49].

Optogenetic stimulation possesses key advantages over the already established electrical and pharmacological forms of stimulation. Electrical stimulation affects all cells at site of stimulation. With the MEA systems, electrodes are in fixed positions, and thus can only stimulate a limited section of a network at a time while also bringing about unwanted associated artifacts [55]. Optical stimulation will only stimulate those cells transduced with the rhodopsin protein. The disadvantages of pharmacological or chemical stimulation are the requirement for continuous or repeated treatments, sacrificing the ability for temporal control and likely impeding with the physiological environment of the cells [56].

Previously stated, neural plasticity plays an important role in neural networks. Optogenetics have been used as an external stimulus to test neural plasticity and view the results on an MEA [11]. Tests to study both long-term and adaptive plasticity of the neuronal culture through light exposure at varied intervals for particular lengths of time on primary mouse hippocampal neurons, transduced with ChR2 via a lenti-viral system,

demonstrated how the networks adjusted to different stimulation approaches [11].

Mature networks display intrinsic spontaneous bursting and firing patterns, while neurological diseases, such as epilepsy and Parkinson's are associated with abnormal increases in such patterns [57]. Imagine being able to attenuate episodic seizures by inducing a pattern correction through optical stimulation. Specific conditions of optogenetic stimulation can amply generate network-wide changes to burst and synchrony patterns, which ultimately lead to network reorganization. These results proved the potential for using optogenetics as a tool for developing epileptic or other neurological disease models [58]. Combining both optogenetic and MEA technology opens up a lot of possibilities for studying the electrophysiological responses and functions of neural networks [11, 58]. With the utilization of stem cells supplying a bottomless reservoir of cells that possess the capability to differentiate into relevant neural lineages, the applications of this technology to study neural network function become almost limitless.

6. ELECTROPHYSIOLOGICAL ANALYSIS OF OPTICALLY ACTIVE STEM CELL DERIVED MOUSE NEURAL NETWORKS

Introduction

Movement, learning, and memory, just to name a few, are complex and essential abilities for both animals and humans. Unfortunately, there are almost infinite means that can result in their malfunction. Understanding the finite details of the mechanisms of these abilities is a difficult but necessary task. Although live animal experiments would provide the most powerful tool for accomplishing such a difficult task, it is far from the most efficient. In vitro models for in vivo mechanisms not only provides a more cost effective means, but also provides an ethical advantage from not having to sacrifice so many live animals. The application of embryonic stem cells provides an infinite source of cells with the capability to differentiate into a plethora of neural cell types.

The capacity for limitless neurons and neural networks in vitro establishes the platform to test the functionality of said networks. Microelectrode Array

(MEA) technology provides the means for demonstrating and manipulating the functionality of neural networks *in vitro* due to its ability to monitor firing, bursting, and synchronic activity. Recording network activity on the MEA does not harm the networks, thus allowing for multiple recordings from the same sample over extended periods of time [19]. Stem cell derived cortical and motor neural networks have proven to resemble the electrophysiological and pharmacological functionality of primary cultures [10, 20, 33].

By inserting the genes of light-sensing rhodopsin proteins into neurons, optogenetics provides an outlet for further analysis and manipulation of cellular activity [51]. Neurons genetically modified to express channelrhodopsin-2 stimulated and plated on the MEA demonstrated the capability to alter network plasticity [11], bursting patterns, and even network synchronization [58] of when stimulated with specific patterns using blue light. Their results verified that optogenetics can be used to manipulate and control the advanced electrophysiological attributes of *in vitro* neural networks.

In this study, we combine the above strategies to assess the optical and pharmacological functionality of optically active stem cell derived neural networks on the MEA system. Because previous studies have demonstrated the ability to modify network activity [11] with optogenetics we hypothesized that when exposed to blue light, channelrhodopsin-2 (ChR2) integrated neural networks would respond with an increase in activity at time of exposure. Previous studies have also shown that stem cell derived neural networks respond to pharmacological reagents similarly to primary cultures. As a result, we hypothesized that we could characterize functional neurotransmitter activity of mouse embryonic stem cells differentiated towards motor neurons after exposure to several pharmacological reagents. The results demonstrated that when network activity including mean firing rate and synchrony increased when exposed to blue light. Pharmacological experiments validated proper functionality of both gamma-aminobutyric acid (GABA) and glutamate receptors. We saw the expected changes in network activity after GABA, 2-amino-5-phosphonovalerate (AP5), N-methyl-D-aspartic-acid (NMDA), α -amino-3-hydroxy-5-methyl-4-isoxazole propionic acid (AMPA), and bicuculline treatments. Our study establishes this cell line as a functional model for more advanced optical and pharmacological experiments.

Experimental Procedures

Differentiation of Mouse Embryonic Stem Cells

HBG3 Rosa26-ChR2 mouse embryonic stem cells (mESCs) were generously donated by the Kamm lab at MIT. Channel rhodopsin-2 (ChR2), a blue light activated positive transmembrane protein, was integrated through nucleofection into the Rosa26 locus to be constitutively expressed (**Figure 6.1A**). This cell line also contains linked expression of GFP and HB9, a motor neuron specific marker, to visualize motor neurons. The mESCs were directed towards motor neuron differentiation following a 7-day differentiation protocol. Mouse ESC's were plated on a cell culture dish and incubated on a shaker to induce formation of spherical embryoid bodies (EB's) (**Figure 6.1B**). Neural differentiation media contained Advanced DMEM F12 (Gibco), AB2 Neural Basal Media (ArunA Biomedical), Knock-out Serum (Gibco), Pen/Strep (Gibco), L-Glutamine, and B-me (Gibco). Media changes were conducted on Day's 1, 2, 3, and 6. Days 2, 3, and 6 included the addition of 1 μ M of Retinoic Acid (Sigma) and 1 μ M of Purmorphamine (Calbiochem), a Sonic hedgehog agonist, to induce motor neuron differentiation. Day 6 also included the addition of 10ng/ml of GDNF (Neuromics) and BDNF (R&D Systems) for neural survivability. On Day 7,

EB's were collected and dissociated to plate as a monolayer. After dissociation, cells were immediately plated or frozen in Cryostor (Sigma).

MEA System and Multi-well Plates

This experiment used Axion's Maestro MEA system (Axion Biosystems). Black ANSI compliant well MEA plates (Axion Biosystems) consisted of 48 wells containing 16 nano-textured gold electrodes (~40-50 μm diameter) each totaling 768 channels. Cells were unable to be viewed through microscopy.

MEA Surface Pretreatment

The procedures followed Axion's ArunA Biomedical mMNGFP+ Mouse Motor Neurons GFP+ Culture Protocol. A 0.1% Polyethylenimine (PEI) (Sigma) solution was prepared with Boric Acid (J.T.Baker) and Sodium Tetraborate (J.T.Baker) in sterile DI water. 5 μL droplets of the 0.1% PEI solution were then added on top of the electrode area to each of the wells. Sterilized water was added to the area surrounding the wells to avoid substrate evaporation. PEI treated plates were then incubated at 37°C for 1 hour. After incubation, the PEI droplets were rinsed with sterile DI water 4 times and allowed to air dry in the biological safety cabinet overnight. Fresh

laminin (Sigma) solution was prepared in AB2 at a concentration of 20 μ g/ml and added as 5 μ L droplets on top of the MEA's electrode areas and plates were incubated at 37°C for 2-4 hours. Excess laminin was removed before cells were plated. 5 μ L droplets were used to ensure cell adhesion to electrode area (**Fig 6.1C**).

Seeding and Maintenance of Cells on the MEA

Differentiated cells were plated in 5 μ L droplets on top of the electrodes at 80,000 cells per well (**Figure 6.1D**). Cells were given a 1-hour incubation period to plate down followed by an addition 300 μ L of neural differentiation media (with GDNF and BDNF) added in two 150 μ L aliquots to each well to avoid detachment of cells. Any excess water in surrounding areas was removed. Half media changes (with GDNF and BDNF) were conducted every 2-3 days.

MEA Recordings

Recordings were taken on Axion's Integrated Studio (AxIS 2.0) program with the manufacturers recommended settings for recording neural activity. This included a butterworth band-pass filter (200–3000 Hz) and a threshold spike detector set at 6x standard deviation of the rms noise to reduce false

positives as a result of ambient noise. Data was saved in 3 different file types; a raw data file (*.raw file) that included all data and a spike file (*.spk file) that included spike and bursting metrics were recorded simultaneously, and a neural metrics file (*.csv file, recorded post hoc) that included addition variables such as network burst percentage. Activity recordings, including pharmacological and optical stimulations, were conducted on DIV8, 13, and 17 to explore possible developmental changes to network activity and stimuli response. Recordings each day started with 5 minutes to allow plates to equilibrate followed by a 5-minute recording of basal activity.

Pharmacological Stimulation

Designated wells were treated with AMPA (1 or 5 μ M, Sigma), AP5 (50 μ M, Sigma), Bicuculline (50 μ M, Sigma), GABA (100 μ M, Sigma), Glycine (100 μ M, Bio-Rad), or NMDA (40 μ M, Sigma). Required reagents were dissolved in <0.01% dimethylsulfoxide (DMSO, Sigma). Reagents were reconstituted and stored as per manufacturers recommendations. All reagents were diluted in AB2 neural basal media to avoid major osmotic changes when added to cultures. Frozen reagents were stored in aliquots to avoid repeated freeze-thaw cycles. Treated wells were given 15 minutes to allow for temperature

adjustments and compound equilibration followed by a 5-minute recording. Wells treated with DMSO (control), GABA, AP5, and NMDA were also treated with their antagonists, Bicuculline, NMDA, and AP5. Subsequently added compounds received an additional 15-minute equilibration period and 5-minute recording.

Optical Stimulation

Wells designated for optical stimulation were exposed to blue-light (~470nm) using an LED curing light (UltraLume LED5). Nearby wells were covered to limit exposure. Optical stimulation was composed of 5-minute recordings starting with a 1-minute recording of basal activity followed by 2 different stimulation patterns lasting 1 minute each. Patterns were chosen for clear visualization of activity response and followed by 1 minute of no stimulation. Pattern 1 consisted of a repeated 2 seconds of exposure with 5-second breaks for 1 minute. Pattern 2 consisted of a repeated 10 seconds exposure with 10-second breaks for 1 minute.

Data Analysis

Data was collected from 3 separate experiments. Wells were used as the unit of measurement; an individual well was considered an observation ('n')

for all analyses. Active wells, defined as having 8 or more active electrodes, were determined from baseline recordings each day. An active electrode was one that recorded 5 or more spikes/min with an rms-noise level below $10\mu\text{V}$ [26]. Electrodes with rms-noise levels above $10\mu\text{V}$ were turned off. Wells that did not meet these requirements were excluded from the data. AxIS Spike files were uploaded to Neuroexplorer 4 (NEX Technologies) and used to perform burst and mean firing rate (MFR) analysis. A burst was defined as having a maximum of 0.01s interval to start burst and 0.075s to end burst with a minimum of 4 spikes lasting 0.02s with 0.1s between bursts (recorded in 0.02s bins) [19].

Axion's Neural Metrics Tool was used for network burst and synchrony metrics as well as the creation of raster plots and cross-correlograms. Blue on the raster plots denotes bursts while the magenta boxes denote network bursting. Bursting parameters were set at a minimum of 4 spikes/min with a max interspike interval (ISI) threshold of 100 ms. Network burst parameters were set at min of 10 spikes with an adaptive ISI threshold [22]. To analyze synchrony, the synchrony window was set to 25 ms [21] and synchrony was measured by the area under normalized cross-correlograms with a larger area indicating increased synchronous firing.

Neural metric variables were calculated for both the basal and treated electrodes. Due to variability within treatments, well averages for each variable were weighted by total number of active electrodes using EXCEL's SUMPRODUCT function and averaged across the total sum of active electrodes to receive a final weighted average. Tables display weighted averages \pm SE of the mean (SEM).

Significance was determined by paired-samples t-test for individual treatments. One-Way ANOVAs with LSD post hoc analyzed changes by day. A *p* value of less than 0.05 was considered to be statistically significant. For calculation of percent change over time for statistical analysis, zeroes were changed to 0.0001 to avoid division by zero.

Results

HBG3 Neural Network Development

As expected, we observed increased activity as the network matured (**Figure 6.2A**). From DIV8 to DIV13 mean firing rate (MFR), bursts per min, burst duration, mean frequency in bursts network burst percentage, and synchrony (**Table 6.1**). However, spiking and bursting activity seemed to

have peaked by DIV13. Between DIV8 and DIV17, synchrony was the only metric that increased significantly (**Figure 6.2B**).

Network Responses to Pharmacological Treatments

Pharmacological treatments were conducted for characterization of network properties of the mixed neural culture. Treatments were carried out on days 8, 13, and 17 post plate. The plates were allowed 5 minutes of calibration before a 5 min basal recording was measured. Pharmacological treatments were added and given 15 min to equilibrate before measuring a 5 min response recording.

Although DMSO initially displayed minimally inhibitory affects, network activity recovered by 40 minutes after application (Table). DMSO treatments were terminated after DIV13.

To assess excitatory glutamate responses, cultures were treated with either N-methyl-D-aspartic-acid (NMDA, 40 μ M) or α -amino-3-hydroxy-5-methyl-4-isoxazole propionic acid (AMPA, 1 μ M or 5 μ M). NMDA increased activity on all days with diminished effects by DIV17 (**Figure 6.3**). NMDA tended to disrupt network synchrony with a significant decrease on DIV13 and lower

the mean frequency in burst with a significant decrease seen on DIV17 (Table 6.3). Addition of antagonist 2-amino-5-phosphonovalerate (AP5) to NMDA treated decreased all neural metrics (Figure 6.4) with significant decreases in mean firing rate, mean frequency in burst, and network burst percentage on DIV8 and 13. Significant decreases in bursts per minute and synchrony was also observed in DIV8 (Table 6.3). AP5 treatments had significant percent changes between DIV8 and DIV13 for bursts per minute and mean frequency in burst (Table 6.3), DIV8 and DIV17 for mean frequency in burst and network burst percentage, and DIV13 and DIV17 for mean firing rate and network burst percentage (Table 6.3).

General decreases in activity followed individual AP5 treatments (Figure 6.4). Significant decreases were witnessed in mean firing rate, bursts per minute, and network bursts on DIV8 (Table 6.4). AP5 displayed significant decreases in all metrics but synchrony on DIV13 (Table 6.4) and all metrics but burst duration and network burst percentage on DIV17 (Table 6.4).

AMPA (5 μ M) exhibited extremely excitotoxic effects with obvious activity inhibition (Figure 6.5). We observed almost complete elimination of activity with AMPA (5 μ M) treatments (Tables 6.5). As a result, AMPA (5 μ M)

treatments were discontinued after DIV13 to focus on the excitatory affects of a lower concentration.

AMPA (1 μ M) displayed varying affects. On DIV8, AMPA (1 μ M) demonstrated minor inhibitory effects (**Table 6.5**); however, treatments on DIV13 and 17 both showed excitatory responses (**Figure 6.5**) with significant increases in mean firing rate and mean frequency in bursts seen on DIV13 (**Table 6.5**).

GABA (100 μ M) displayed significant inhibitory effects (**Fig 6.6**). Significant decreases were observed in almost all metrics on all days (**Table 6.6**).

Subsequent treatment with the GABA_A receptor antagonist bicuculline (50 μ M) was able to partially restore lost activity as well increase synchronous firing (**Fig 6.6**) with diminishing effects by DIV17 (**Table 6.6**). Addition of bicuculline exhibited significant restoration of mean firing rates on all days (**Table 6.6**).

Independent bicuculline (50 μ M) treatments increased mean firing rates as well as synchronous bursting (**Fig 6.7**). Bicuculline significantly increased all neural metrics except mean burst duration on DIV8 (**Table 6.7**), network

burst percentage and synchrony on DIV13 (**Table 6.7**), and no significant effects on DIV17 (**Table 6.7**). Again, diminished response was observed by DIV17 as soon by significant percent change differences in synchrony and mean burst duration from DIV8 (**Table 6.7**).

Glycine (100 μ M) treatments surprisingly displayed excitatory effects on DIV13 and 17 (**Figure 6.8**). Significant increases in mean firing rate were recorded on DIV13 and DIV17 (**Table 6.8**). Similarly to NMDA, glycine caused a decrease in network synchrony with significant decreases on DIV8 and DIV13 (**Table 6.8**).

Increased Network Firing from Optical Stimulation

Within a 5-minute recording, cultures were exposed to blue light at 2 different stimulation patterns separated by a 1-minute resting period. The stimulation pattern consisted of a repeated 2 seconds of exposure followed by 5 seconds rest, while the second pattern was comprised of repeated 10 seconds of exposure followed 10 seconds of rest. Non-ChR2 HBG3 networks were optically stimulated as a negative control. Blue light stimulation increased activity on DIV8 and 13 showing visible peaks at times of exposure (**Fig 6.9**). Stimulation on DIV8 resulted in significant increases in synchrony

(**Table 6.9**). Significant increases in mean firing rate and burst duration were observed in both stimulation patterns on DIV13 (**Table 6.9**). However, stimulation on DIV17 showed no significant effect on any metric with significant decreases in percent changes between DIV17 in mean firing rate during both stimulation patterns (**Table 6.9**). No significant affects were seen in non-ChR2 HBG3 networks.

Discussion

In this study we plated HBG3 ChR2 mouse neurons on the Axion Maestro MEA system after a 7-day protocol for motor neuron differentiation. To our knowledge, this is the first time this cell line has been used on an MEA system. We have characterized the spiking and bursting activity of the cultures.

Electrophysiological activity increased over time as the network developed. Network characteristics, such as network bursting appeared as early as 8 days post plating (**Fig 6.2**) with more mature characteristics, such as synchronous bursting, appearing by DIV17 (**Fig 6.2**). Synchronous firing was even observed as early as DIV8 in specific wells (data not shown). This is earlier than what has previously been seen by ES-derived neural networks

with synchronous bursting only appearing after 28 days in culture [33]. This indicates that the HBG3 networks reach developed states earlier than other stem cell derived neural networks; advantageous for using as a model for studying mature network characteristics.

Pharmacological characterizations of the network activity demonstrated significant decreases in activity from GABA treatments. Bicuculline treatments partially restored activity lost by GABA, and independent treatments increased bursting rates and network bursts as well as inducing or increasing synchronous bursting. Our results were consistent with what has been seen in ESC-derived neural networks and both primary hippocampal and motor neuron cultures [33, 59].

We also observed modulation of network activity by NMDA (40 μ M) treatments and its antagonist AP5 (50 μ M). NMDA treatments increased firing rates and addition of AP5 greatly decreased activity metrics. These results are consistent with what has been previously seen in both primary rat spinal neurons and human ES derived neural networks [24] as well as NMDA's reduction of synchronous activity has been recorded in ES derived neural networks [33].

AMPA (5 μ M) had an extremely excitotoxic effect causing a significant reduction of activity, while AMPA (1 μ M) showed excitatory effects on DIV13 and 17 with no significant effect on DIV8. Lower concentrations of AMPA exhibited excitotoxic effects imply that these cultures exhibit a higher sensitivity to AMPA than NMDA. This is most likely due to the activated of AMPA receptors opening both AMPA and NMDA channels. At resting membrane potential, Mg²⁺ blocks the passage of permeable ions through NMDA channel. Mg²⁺ is released by a depolarization of the membrane. Therefore, by depolarizing the membrane through AMPA receptors, NMDA receptors are also activated [13]. Previous studies have used an NMDA antagonist, such as AP5, to focus on AMPA's influence on activity [58]. For future experiments, this would be a more prudent approach for analyzing AMPA-mediated activity.

The differentiation protocol to for motor neuron differentiation involves the addition of Sonic hedgehog and Retinoic Acid, two key regulators necessary for spinal fate induction. As one of the primary inhibitor neurotransmitters in the spinal cord, we expected to see a decrease in activity with the application of glycine [40] However, we observed the opposite with

increases in activity on DIV13 and 17. This data suggests a lack-of inhibitory glycine receptors in the network and the resulting increase of activity is most likely due to glycine contributing to its role as a co-agonist for the excitatory glutamate NMDA receptor [32].

Optical stimulation with blue LED elicited increased network activity and bursting metrics during exposure on DIV8 and 13. The channel rhodopsin-2 (ChR2) gene was inserted onto the Rosa26 locus. Rosa26 is expressed in all cell types and is a common gene target for genetic engineering as it is protected from silencing, thus being constitutively expressed. This implies that exposure to blue light opens all ChR2's positive ion-gated channels theoretically exciting every cell type. Increased activity at time of exposure indicates that in this culture excitatory neurons have a larger influence on network activity. ChR2 has been specifically integrated into GABAergic neurons by targeting the gene for the vesicular GABA transporter (VGAT) creating chimaera mice. Blue light exposure at specific locations on the mice's spinal cord inhibited mouse hind or fore limb movement [54] showing that the excitatory signals from activated ChR2 channels can induce inhibitory effects. Our results suggest that the composition of these cultures might consist of a larger percentage of excitatory neurons over inhibitory.

In conclusion, motor neuron differentiated networks derived from embryonic stem cells display properties seen by a range of primary neural cultures and other ES derived networks, including glutamate receptor activation by NMDA, AP5, AMPA, and glycine, as well as inhibition by GABA. These networks also possess the ability optical stimulation granting the potential for more advanced light stimulation experiments, such as synchrony or plasticity manipulation. Although results and trends were observed, evident variation and a lack of statistical significance designate a need for further investigation. However, this study validates the budding talent and potential of combining MEA and ontogenetic with this culture to use as potential models for network properties and eventually degenerative diseases.

Acknowledgements

I greatly appreciate and thank EBICS for their financial support of this research. I would also like to thank Sebastian Uzel at the Kamm Lab at MIT for generously supplying the Chr2 mESC's used for these experiments as well as Axion Biosystems and the Shafer lab for their technical support and assistance on MEA related matters. Finally, I'd like to extend a special thanks to Erin Jordan and Colette Miller for the teaching of and assistance with experimental procedures.

Figure 6.1:

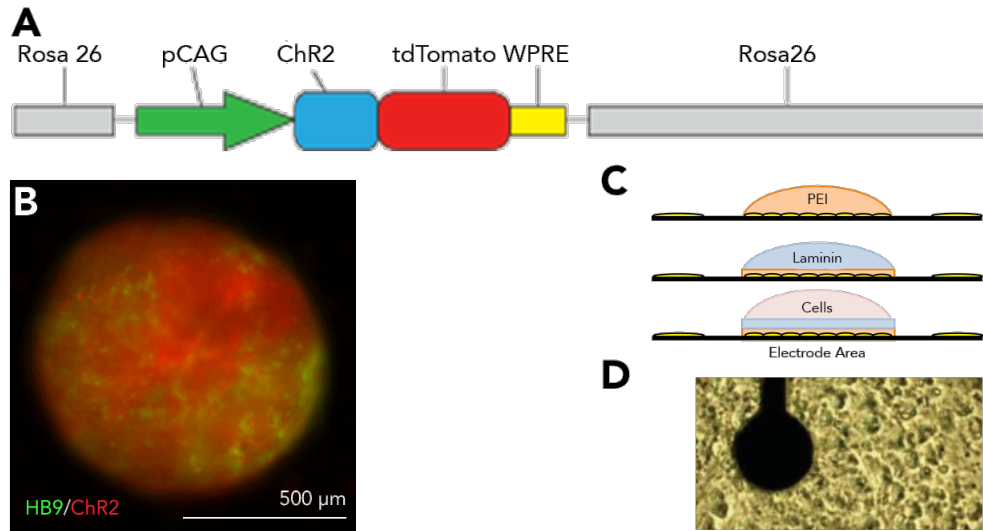


Figure 6.1: Experimental Set-Up

(A) Diagram of gene construct. Using pCAG as the plasmid vector channelrhodopsin-2 (ChR2) was inserted into the protected Rosa26 locus via nucleofection along with tdTomato for visualization and Woodchuck hepatitis post-transcriptional regulatory element (WPRE) for enhanced gene expression. (Adapted from Kamm lab) **(B)** Image of day 7 embryoid body. GFP denotes cells expressing HB9, a motor neuron marker. RFP denotes cells expressing ChR2. **(C)** Diagram of droplet protocol displaying application of polyethyleneimine (PEI) followed by laminin and finally the cells. **(D)** Image of HBG3 mouse motor neurons plated at 60,000 cells on MEA plate (DIV6, Adapted from Axion Biosystems).

Figure 6.2:

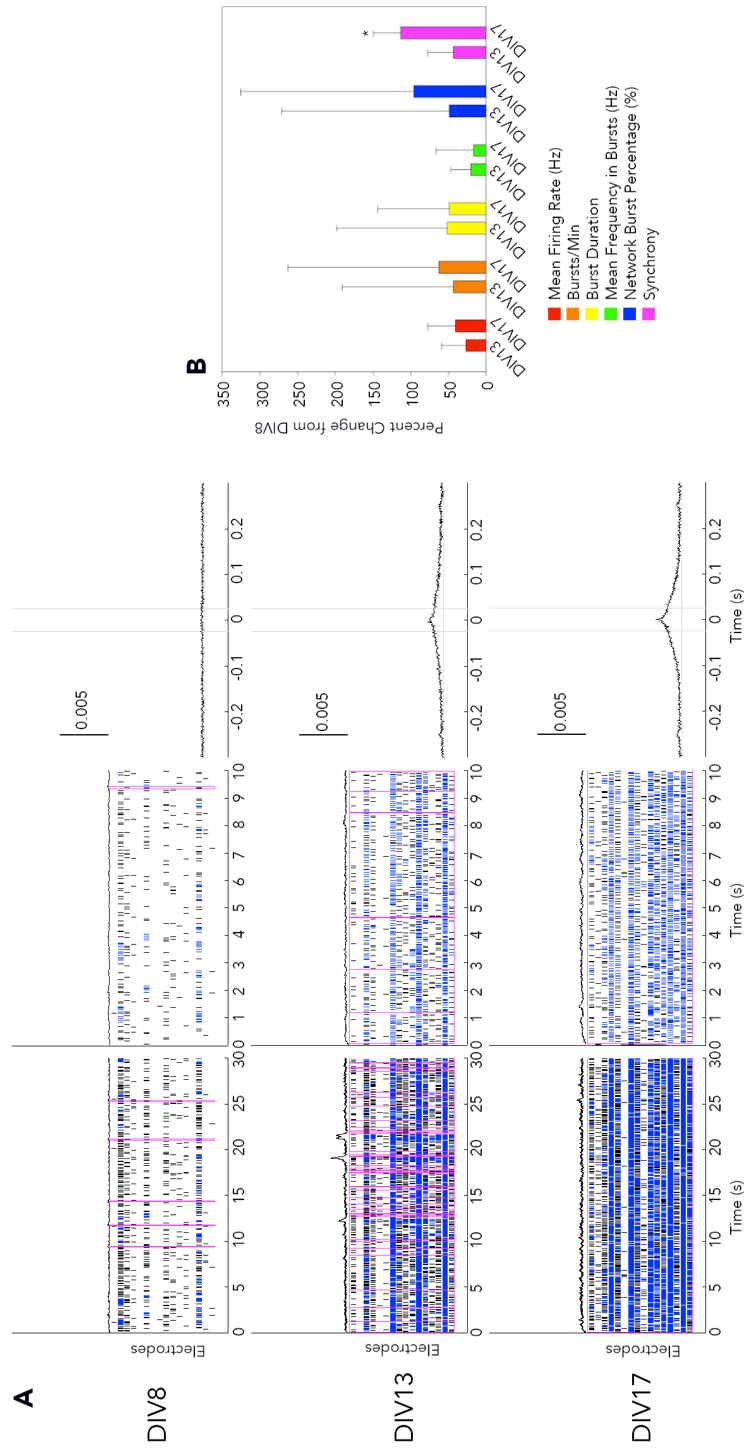


Figure 6.2: Developmental Changes of HBG3 ChR2 Neural Networks

Raster plots on all days display the activity progression from the same well. Blue bars indicate single channel bursts. Pink boxes outline network bursts.

(A) Raster and normalized cross-correlograms of spontaneous activity of DIV8, 13, and 17 respectively from the same well. Left images are 30 sec plots. Middle images are the first 10 sec of the 30 sec plots. **(B)** Graph of percent change of measured neural metrics from DIV8. Data are the mean percent change from DIV8 \pm SEM.

**p*<0.05

Table 6.1: Developmental Changes of HBG3 ChR2 Neural Networks

	Mean Firing Rate (Hz)	Bursts/Min	Mean Burst Duration (s)	Mean Frequency in Bursts (Hz)	Network Burst Percentage (%)	Synchrony
DIV8 (n=8)	3.893 ± 0.434	3.496 ± 0.974	0.082 ± 0.018	21.024 ± 3.631	32.249 ± 9.578	0.032 ± 0.006
DIV13 (n=7)	5.367 ± 0.912	6.197 ± 2.040	0.171 ± 0.077	26.604 ± 4.768	63.607 ± 14.519	0.057 ± 0.010
DIV17 (n=5)	5.488 ± 1.148	5.695 ± 1.283	0.123 ± 0.053	24.502 ± 4.090	63.253 ± 15.482	0.069 ^b ± 0.016

Values are displayed as weighted averages ± SEM

^aSignificant percent change from DIV8 to DIV13 ($p < 0.05$)

^bSignificant percent change from DIV8 to DIV17 ($p < 0.05$)

Table 6.2: DMSO Results

DMSO		Mean Firing Rate (Hz)	Bursts/Min	Mean Burst Duration (s)	Mean Frequency in Bursts (Hz)	Network Burst Percentage (%)	Synchrony
DIV8 (n=5)	Basal	4.56 ± 0.63	4.97 ± 1.97	0.10 ± 0.02	29.56 ± 6.77	47.02 ± 13.75	0.07 ± 0.03
	DMSO	3.46* ± 0.73	3.46 ± 1.79	0.11 ± 0.03	30.41 ± 9.33	20.78 ± 13.02	0.07 ± 0.03
	40 min Post (n=3)	6.27 ± 0.39	7.76 ± 2.59	0.09 ± 0.03	28.45 ± 10.30	73.20 ± 26.56	0.05 ± 0.02
DIV13 (n=3)	Basal	5.69 ± 0.76	4.97 ± 1.97	0.06 ± 0.01	24.28 ± 10.06	63.02 ± 18.20	0.06 ± 0.01
	DMSO	4.35 ± 0.07	3.46 ± 1.79	0.05 ± 0.02	16.70 ± 5.33	27.88 ± 9.55	0.03 ± 0.01
	40 min Post	4.94 ± 0.58	8.40 ± 1.80	0.04 ± 0.01	16.45 ± 5.22	56.26 ± 15.18	0.04 ± 0.01

Values are displayed as weighted averages ± SEM

**Significant change (p<0.05)*

Figure 6.3:

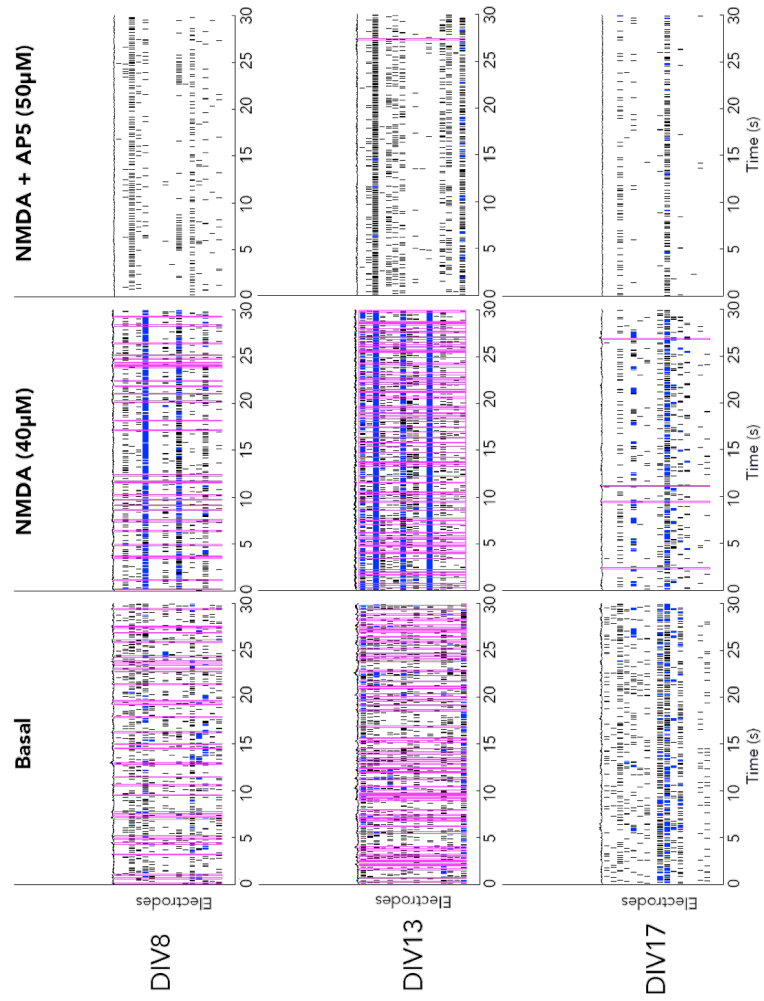


Figure 6.3: NMDA Raster Plots

Raster plots follow the same well by treatment, but not by day. Blue bars indicate single channel bursts. Pink boxes outline network bursts. Cultures were treated with NMDA (40 μ M) on DIV8, 13, and 17. After initial NMDA treatment, cultures were treated with NMDA antagonist AP5 (50 μ M). NMDA treatments increased firing, bursting, and network bursting, while addition of AP5 decreased the effects.

Table 6.2: NMDA Results

NMDA (40 μ M)		Mean Firing Rate (Hz)	Bursts/Min	Mean Burst Duration (s)	Mean Frequency in Bursts (Hz)	Network Burst Percentage (%)	Synchrony
DIV8 (n=9)	Basal	3.132 \pm 0.402	2.894 \pm 1.166	0.064 \pm 0.013	23.091 \pm 4.943	23.490 \pm 8.272	0.05 \pm 0.02
	NMDA	3.93 \pm 0.41	2.65 \pm 0.66	0.12 \pm 0.04	19.63 \pm 5.41	17.58 \pm 4.58	0.02 \pm 0.01
	NMDA + AP5	0.86* \pm 0.12	0.02* \pm 0.02	0.02 \pm 0.02	1.80* \pm 1.09	0*	0.01* \pm 0.00
DIV13 (n=8)	Basal	3.23 \pm 0.56	2.18 \pm 0.74	0.05 \pm 0.01	18.58 \pm 4.48	26.92 \pm 8.79	0.04 \pm 0.01
	NMDA	4.97 \pm 0.82	2.57 \pm 0.62	0.21 \pm 0.08	9.71 \pm 0.89	40.78 \pm 14.11	0.02* \pm 0.00
	NMDA + AP5	2.28* ^a \pm 0.25	1.52 ^a \pm 0.77	0.02 \pm 0.01	3.50* ^a \pm 0.74	0.22* \pm 0.10	0.01 \pm 0.00
DIV17 (n=3)	Basal	2.46 \pm 0.64	1.19 \pm 0.89	0.03 \pm 0.01	14.08 \pm 2.34	0.46 \pm 0.20	0.03 \pm 0.01
	NMDA	2.57 \pm 0.86	1.26 \pm 0.59	0.02 \pm 0.01	6.49* \pm 3.04	1.88 \pm 1.16	0.02 \pm 0.01
	NMDA + AP5	1.03 ^c \pm 0.14	0.08 \pm 0.06	0	1.51 ^b \pm 1.24	0 ^{bc}	0.01 \pm 0.00

Values are displayed as weighted averages \pm SEM

*Significant change ($p < 0.05$)

^aSignificant difference in percent change between DIV13 and DIV8 ($p < 0.05$)

^bSignificant difference in percent change between DIV17 and DIV13 ($p < 0.05$)

^cSignificant difference in percent change between DIV17 and DIV8 ($p < 0.05$)

Figure 6.4:

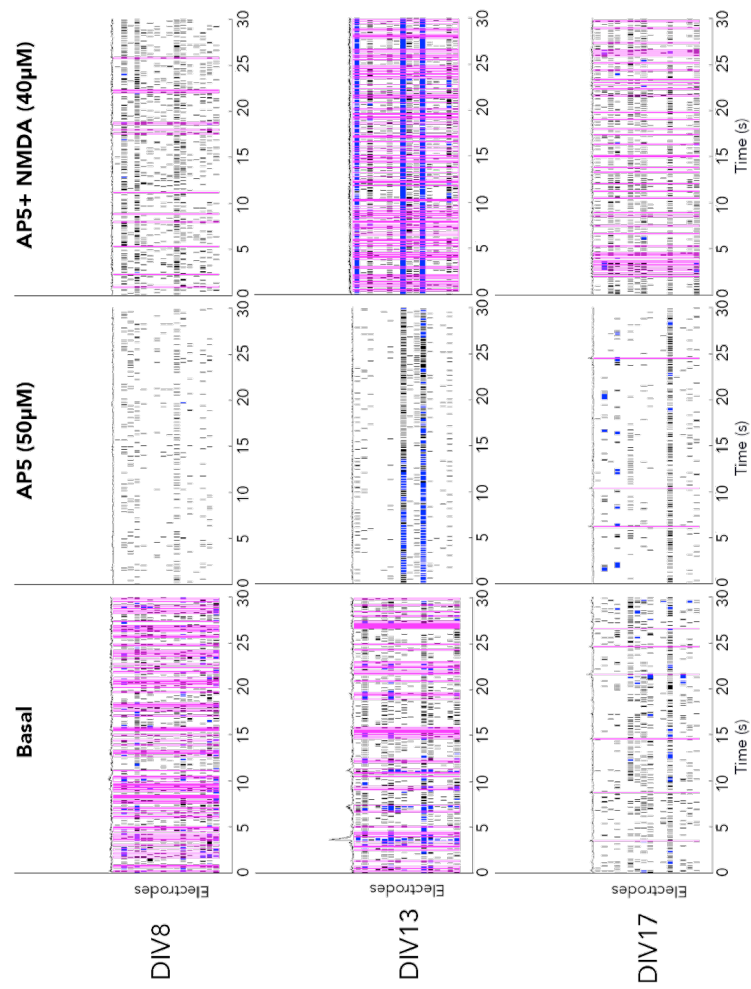


Figure 6.4: AP5 Raster Plots

Raster plots follow the same well by treatment, but not by day. Blue bars indicate single channel bursts. Pink boxes outline network bursts. Cultures were treated with AP5 (50 μ M) on DIV8, 13, and 17. After initial AP5 treatment, cultures were treated with NMDA antagonist NMDA (40 μ M). AP5 treatments decreased network activity, but subsequent treatments with NMDA restored lost activity.

Table 6.3: AP5 Results

AP5 (50 μ M)	Mean Firing Rate (Hz)	Bursts/Min	Mean Burst Duration (s)	Mean Frequency in Bursts (Hz)	Network Burst Percentage (%)	Synchrony	
DIV8 (n=11)	Basal	3.52 \pm 0.59	3.50 \pm 0.98	0.11 \pm 0.03	30.21 \pm 5.96	34.49 \pm 9.64	0.09 \pm 0.03
	AP5	0.87* \pm 0.20	0.095* \pm 0.04	0.05 \pm 0.02	14.37 \pm 6.29	9.28* \pm 4.25	0.03 \pm 0.01
	AP5 + NMDA	3.22* \pm 0.54	2.00 \pm 0.67	0.06 \pm 0.02	12.87 \pm 2.00	1.60 \pm 0.73	0.02 \pm 0.00
DIV13 (n=10)	Basal	3.76 \pm 0.38	3.63 \pm 1.03	0.09 \pm 0.01	33.68 \pm 7.26	22.39 \pm 8.54	0.08 \pm 0.03
	AP5	1.49* ^a \pm 0.20	0.60* \pm 0.28	0.03* \pm 0.01	4.43* \pm 1.35	1.00* ^a \pm 0.66	0.02 \pm 0.00
	AP5 + NMDA	2.16 \pm 0.48	0.59 \pm 0.24	0.04* \pm 0.02	8.22 \pm 1.96	33.14* \pm 11.49	0.03* \pm 0.00
DIV17 (n=8)	Basal	3.14 \pm 0.78	1.48 \pm 0.45	0.09 \pm 0.04	22.95 \pm 6.99	16.95 \pm 11.75	0.05 \pm 0.01
	AP5	1.31* \pm 0.26	0.46* \pm 0.30	0.02 \pm 0.01	13.36* \pm 6.26	0.99 \pm 0.47	0.02* \pm 0.00
	AP5 + NMDA (n=7)	3.68* \pm 1.02	1.89 \pm 0.89	0.18 \pm 0.12	13.99 \pm 2.22	22.75 \pm 14.19	0.04 \pm 0.01

Values are displayed as weighted averages \pm SEM

*Significant change ($p < 0.05$)

^aSignificant difference in percent change between DIV13 and DIV8 ($p < 0.05$)

^bSignificant difference in percent change between DIV17 and DIV13 ($p < 0.05$)

^cSignificant difference in percent change between DIV17 and DIV8 ($p < 0.05$)

Figure 6.5:

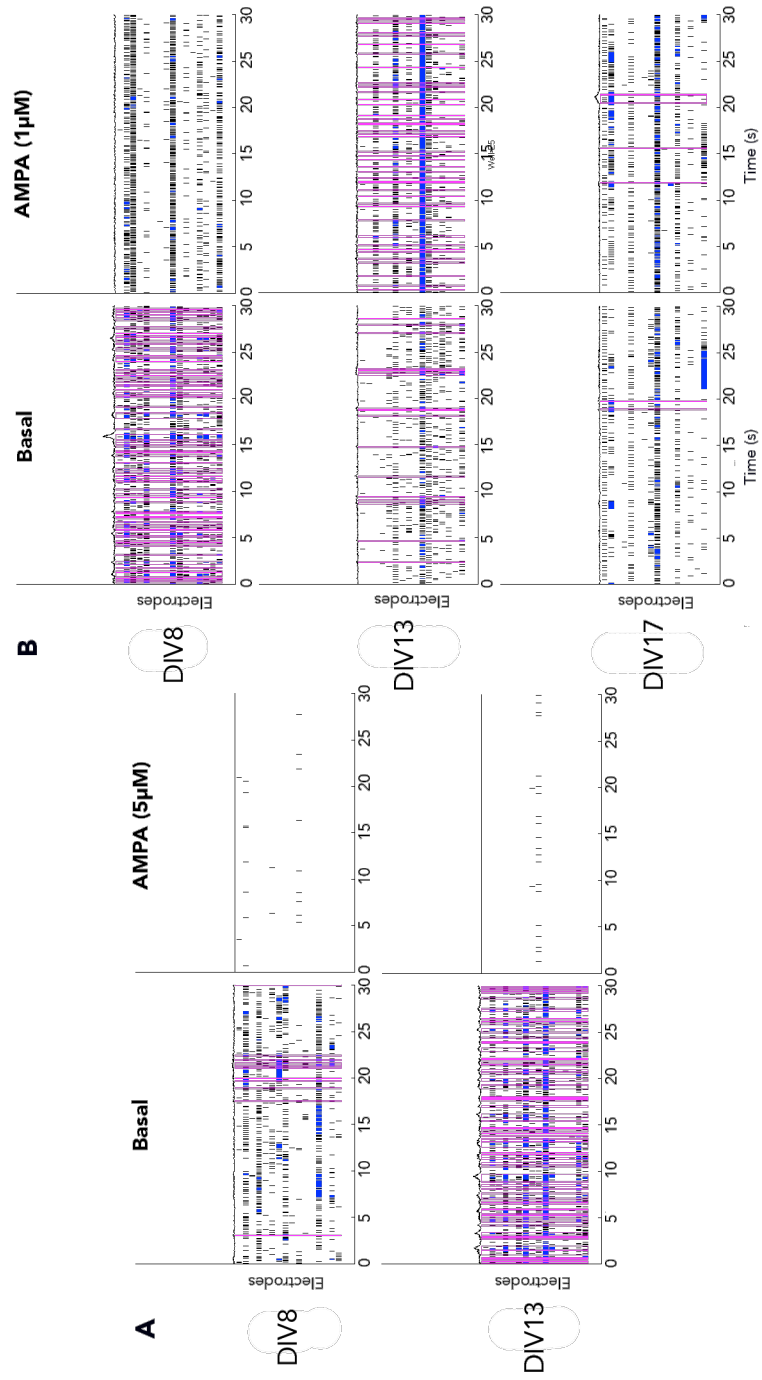


Figure 6.5: AMPA Raster Plots

Raster plots follow the same well by treatment, but not by day. Blue bars indicate single channel bursts. Pink boxes outline network bursts. Cultures were treated with both AMPA (5 μ M) and (1 μ M). 5 μ M displayed excitotoxic effects and resulted in severe activity inhibition. 1 μ M treatments exhibited excitatory effects on DIV13 and 17.

Table 6.4: AMPA Results

AMPA		Mean Firing Rate (Hz)	Bursts/Min	Mean Burst Duration (s)	Mean Frequency in Bursts (Hz)	Network Burst Percentage (%)	Synchrony
DIV8 (5 μ M) (n=4)	Basal	3.17 \pm 0.63	2.44 \pm 1.03	0.10 \pm 0.04	20.87 \pm 5.65	21.00 \pm 12.29	0.02 \pm 0.01
	AMPA	0.02* \pm 0.01	0.01 \pm 0.00	0	10.19 \pm 8.00	0	0
DIV13 (5 μ M) (n=5)	Basal	4.61 \pm 0.31	7.52 \pm 1.77	0.06 \pm 0.01	17.44 \pm 3.37	39.01 \pm 12.29	0.04 \pm 0.01
	AMPA	0.757* \pm 0.480	0.285* \pm 0.289	0.003* \pm 0.003	0.804* \pm 0.817	0*	0
DIV8 (1 μ M) (n=7)	Basal	5.17 \pm 0.99	8.51 \pm 2.70	0.11 \pm 0.02	37.42 \pm 4.64	57.58 \pm 13.41	0.08 \pm 0.02
	AMPA	4.75 \pm 0.97	3.95* \pm 2.17	0.14 \pm 0.04	25.84 \pm 6.25	51.30 \pm 17.12	0.05 \pm 0.02
DIV13 (1 μ M) (n=5)	Basal	3.86 \pm 0.79	5.18 \pm 1.99	0.08 \pm 0.04	24.59 \pm 5.86	31.46 \pm 15.56	0.06 \pm 0.02
	AMPA	4.88* \pm 0.58	6.26 \pm 1.58	0.06 \pm 0.02	12.63* \pm 3.25	52.26 \pm 19.66	0.03 \pm 0.01
DIV17 (1 μ M) (n=5)	Basal	2.98 \pm 0.49	3.61 \pm 2.83	0.19 \pm 0.04	16.55 \pm 3.96	22.66 \pm 9.49	0.02 \pm 0.01
	AMPA	3.86 \pm 0.80	1.62 \pm 0.61	0.10 \pm 0.05	9.40 \pm 2.90	26.04 \pm 18.23	0.02 \pm 0.01

Values are displayed as weighted averages \pm SEM

*Significant change ($p < 0.05$)

^aSignificant difference in percent change between DIV13 and DIV8 ($p < 0.05$)

^bSignificant difference in percent change between DIV17 and DIV13 ($p < 0.05$)

^cSignificant difference in percent change between DIV17 and DIV8 ($p < 0.05$)

Figure 6.6:

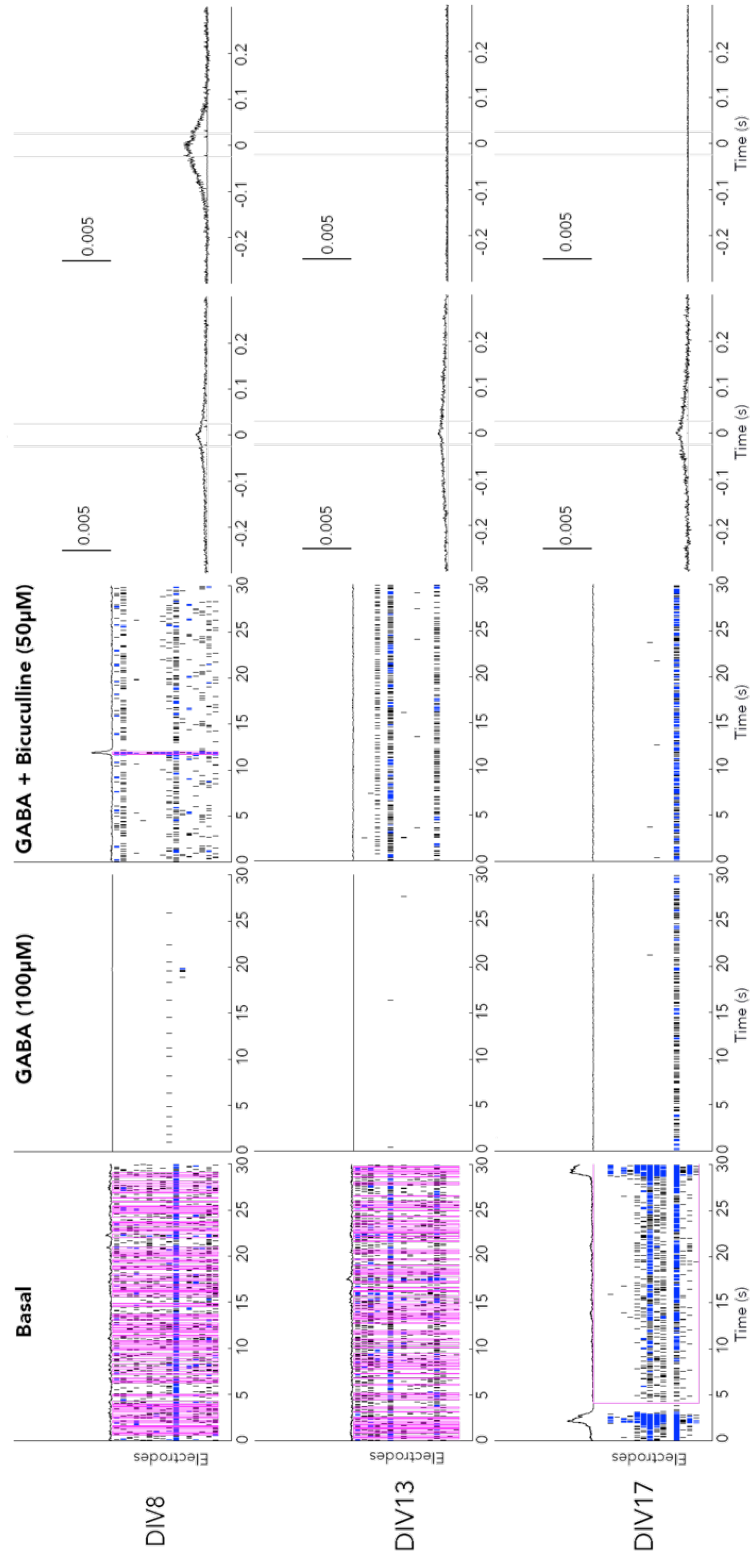


Figure 6.6: GABA Raster Plots

Raster plots follow the same well by treatment, but not by day. Blue bars indicate single channel bursts. Pink boxes outline network bursts. Cultures were treated with GABA (100 μ M) and then subsequently treated with GABA_A antagonist, bicuculline (50 μ M). Bicuculline treatments were able to partially restore activity lost from GABA. Left cross-correlograms show an overlay of basal and GABA synchrony, while right are an overlay of GABA and bicuculline treatments. Bicucullines ability to increase synchrony after GABA treatment decreased on DIV13 and became almost non-existent by DIV17.

Table 6.5: GABA Results

GABA (100µM)	Mean Firing Rate (Hz)	Bursts/Min	Mean Burst Duration (s)	Mean Frequency in Bursts (Hz)	Network Burst Percentage (%)	Synchrony	
DIV8 (n=11)	Basal	5.00 ± 0.66	6.314 ± 1.513	0.13 ± 0.02	35.12 ± 4.38	52.64 ± 11.19	0.09 ± 0.03
	GABA	0.08* ± 0.04	0.10* ± 0.05	0.02 ± 0.01	12.36* ± 4.89	21.25* ± 10.95	0.03* ± 0.01
	GABA+ Bicuculline (n=9)	1.23* ± 0.35	0.78 ± 0.35	0.07 ± 0.03	25.76 ± 11.78	6.25 ± 3.09	0.05 ± 0.03
DIV13 (n=9)	Basal	3.77 ± 0.42	3.04 ± 0.85	0.11 ± 0.02	24.58 ± 3.05	28.10 ± 10.45	0.08 ± 0.03
	GABA	0.34** ± 0.12	0.34* ± 0.31	0.01* ± 0.00	1.70* ± 0.74	0*	0.00* ± 0.00
	GABA+ Bicuculline	1.03* ± 0.22	0.50 ± 0.31	0.03 ± 0.01	6.24 ± 2.63	0.22 ± 0.23	0.01* ± 0.00
DIV17 (n=9)	Basal	3.90 ± 0.40	3.28 ± 0.77	0.16 ± 0.04	33.10 ± 3.44	23.79 ± 11.18	0.07 ± 0.01
	GABA	0.24** ± 0.09	0.04* ± 0.26	0*	0.76* ± 0.40	0	0*
	GABA + Bicuculline	0.56* ± 0.16	0.31 ± 0.26	0.01 ± 0.01	2.63 ± 1.51	0.54 ± 0.61	0.01 ± 0.00

Values are displayed as weighted averages ± SEM

*Significant change ($p < 0.05$)

^aSignificant difference in percent change between DIV13 and DIV8 ($p < 0.05$)

^bSignificant difference in percent change between DIV17 and DIV13 ($p < 0.05$)

^cSignificant difference in percent change between DIV17 and DIV8 ($p < 0.05$)

Figure 6.7:

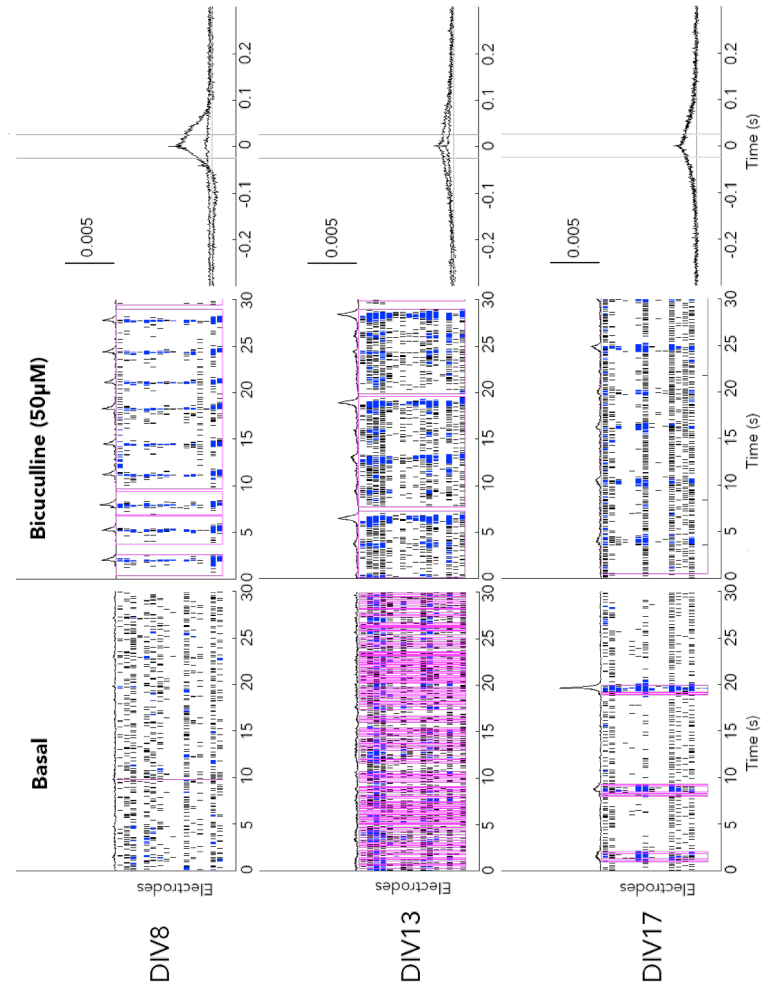


Figure 6.7: Bicuculline Raster Plots

Raster plots follow the same well by treatment, but not by day. Blue bars indicate single channel bursts. Pink boxes outline network bursts. Cultures were treated with bicuculline (50 μ M). Bicuculline increased network activity including induction or increase of synchronous firing. Normalized cross-correlograms display an overlay of basal and bicuculline treatment. Bicuculline treatments increased synchrony but by DIV17 its effect had diminished.

Table 6.6: Bicuculline Results

Bicuculline (50 μ M)		Mean Firing Rate (Hz)	Bursts/Min	Mean Burst Duration (s)	Mean Frequency in Bursts (Hz)	Network Burst Percentage (%)	Synchrony
DIV8 (n=11)	Basal	3.59 \pm 0.55	3.95 \pm 1.33	0.10 \pm 0.01	30.53 \pm 5.24	33.21 \pm 9.97	0.08 \pm 0.02
	Bicuculline	4.77* \pm 0.763	8.31* \pm 1.63	0.18 \pm 0.02	55.50* \pm 10.84	73.10* \pm 10.94	0.21* \pm 0.06
DIV13 (n=9)	Basal	3.83 \pm 0.45	3.13 \pm 0.82	0.09* \pm 0.02	32.76 \pm 10.53	37.87 \pm 10.38	0.07 \pm 0.02
	Bicuculline	4.58 \pm 0.59	4.23 \pm 0.88	0.18 \pm 0.04	41.76 \pm 10.00	63.46* \pm 14.14	0.14* \pm 0.04
DIV17 (n=8)	Basal	2.66 \pm 0.43	1.70 \pm 0.49	0.20 \pm 0.05	21.37 \pm 6.69	23.85 \pm 8.34	0.05 \pm 0.02
	Bicuculline	3.20 \pm 0.62	3.06 \pm 1.13	0.13 ^{bc} \pm 0.02	23.82 \pm 6.33	36.12 \pm 12.38	0.06 ^b \pm 0.02

Values are displayed as weighted averages \pm SEM

*Significant change ($p < 0.05$)

^aSignificant difference in percent change between DIV13 and DIV8 ($p < 0.05$)

^bSignificant difference in percent change between DIV17 and DIV13 ($p < 0.05$)

^cSignificant difference in percent change between DIV17 and DIV8 ($p < 0.05$)

Figure 6.8:

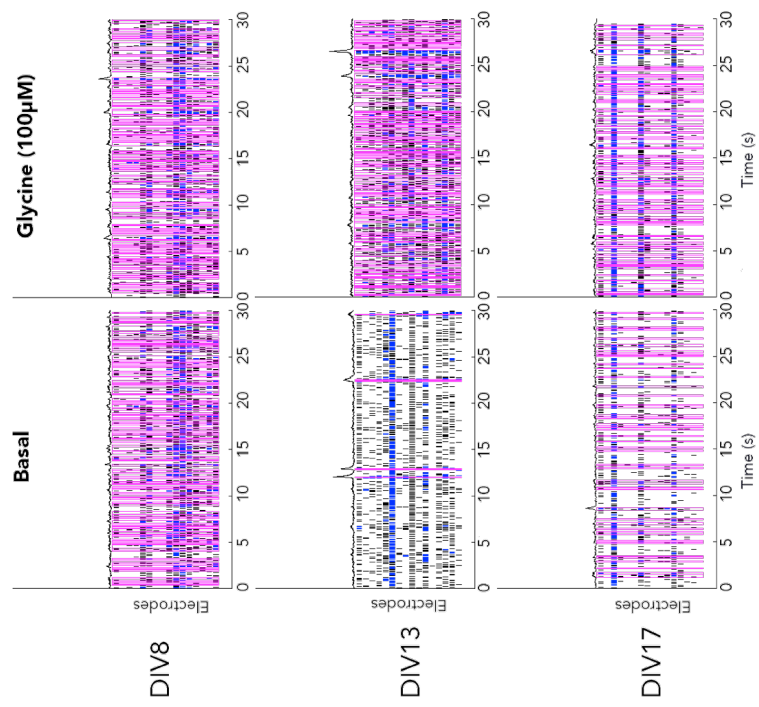


Figure 6.8: Glycine Raster Plots

Raster plots follow the same well by treatment, but not by day. Blue bars indicate single channel bursts. Pink boxes outline network bursts. Cultures were treated with glycine (100 μ M). Glycine showed no obvious effects on DIV8, but exhibited excitatory effects on DIV13 and DIV17.

Table 6.7: Glycine Results

Glycine (100µM)	Mean Firing Rate (Hz)	Bursts/Min	Mean Burst Duration (s)	Mean Frequency in Bursts (Hz)	Network Burst Percentage (%)	Synchrony	
DIV8 (n=14)	Basal	4.46 ± 0.58	5.72 ± 1.18	0.13 ± 0.02	31.46 ± 5.10	48.51 ± 9.62	0.10 ± 0.03
	Glycine	4.85 ± 0.55	6.59 ± 1.34	0.11 ± 0.01	29.44 ± 4.01	49.33 ± 11.02	0.06* ± 0.012
DIV13 (n=10)	Basal	4.01 ± 0.70	5.23 ± 1.41	0.09 ± 0.01	43.57 ± 10.34	26.64 ± 10.42	0.13 ± 0.04
	Glycine	5.21* ± 0.83	5.74 ± 1.57	0.08 ± 0.01	25.18 ± 4.82	52.52 ± 15.45	0.06* ± 0.02
DIV17 (n=9)	Basal	2.88 ± 0.45	3.30 ± 1.44	0.04 ± 0.01	14.95 ± 3.07	19.48 ± 8.07	0.04 ± 0.01
	Glycine	3.78* ± 0.53	4.22 ^{bc} ± 1.34	0.04 ± 0.01	14.06 ± 3.24	26.04 ± 8.74	0.03 ± 0.01

Values are displayed as weighted averages ± SEM

**Significant change (p<0.05)*

^aSignificant difference in percent change between DIV13 and DIV8 (p<0.05)

^bSignificant difference in percent change between DIV17 and DIV13 (p<0.05)

^cSignificant difference in percent change between DIV17 and DIV8 (p<0.05)

Figure 6.9:

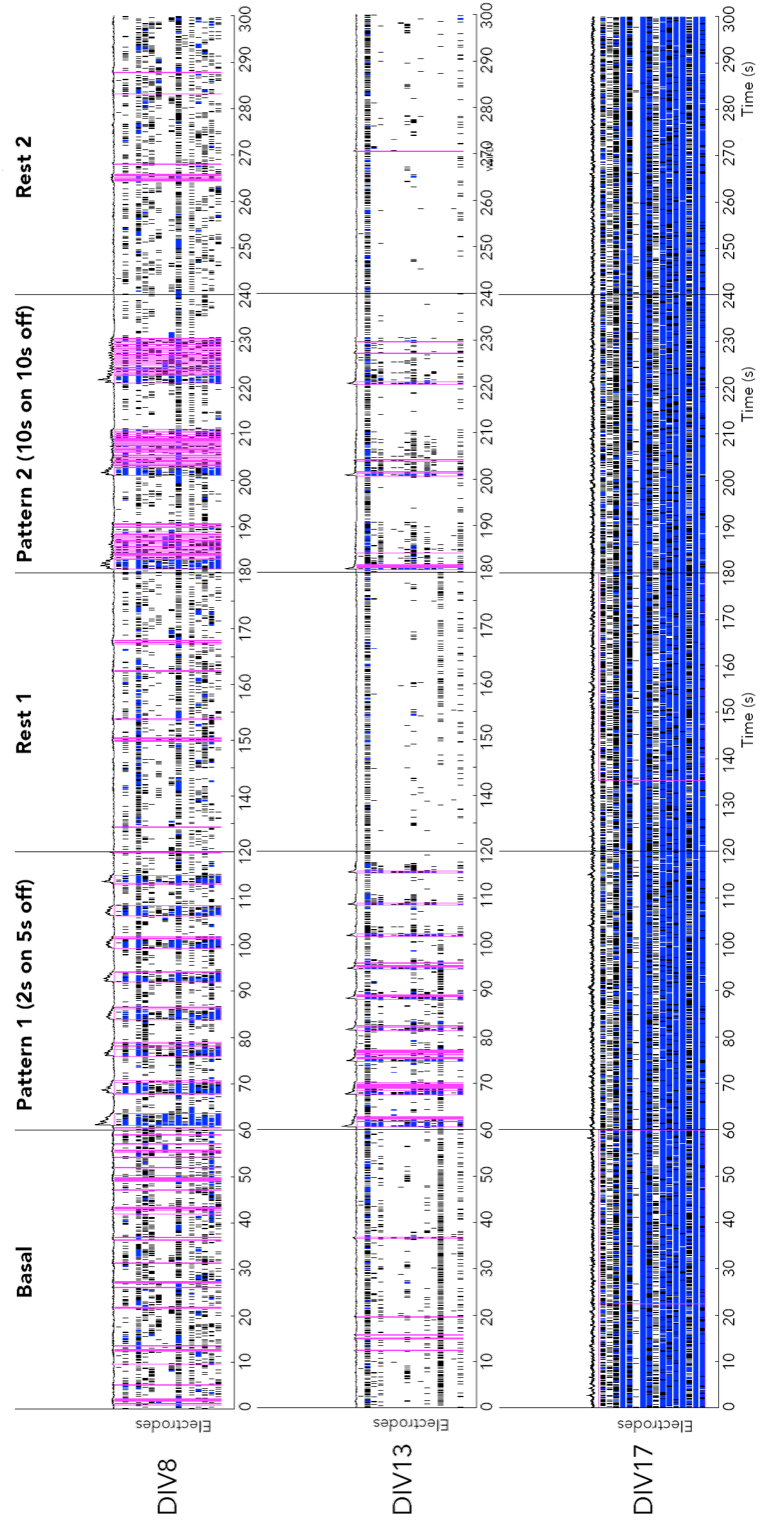


Figure 6.9: Optogenetic Raster Plots

Raster plots follow the same well by treatment, but not by day. Blue bars indicate single channel bursts. Pink boxes outline network bursts. Cultures were exposed to 2 stimulation patterns with 3x60 sec intervals of no stimulation: before, between, and after. Stimulation pattern 1 consisted of 2 sec of exposure 5 sec off intervals for 60 sec. Stimulation pattern 2 consisted of intervals of 10 sec of exposure 10 sec off for 60 sec. On DIV8 and 13 increases in spike rate at time of exposure and can be visualized by spikes on the plots. By DIV17, optical stimulation displayed no obvious affects to activity.

(Rest 1 for DIV8 and 13 was reduced to 50 sec post-hoc due to human error. Stimulation pattern 1 lasted longer than the intended 60 sec)

Table 6.8: Neural Metrics of Optogenetic Stimulation

	60 s Intervals	Mean Firing Rate (Hz)	Bursts/Min	Burst Duration (s)	Mean Frequency in Bursts (Hz)	Network Burst Percentage (%)	Synchrony
DIV8 – Non Chr2 cells (n=3)	Basal	3.16 ± 0.68	2.44 ± 1.71	0.03 ± 0.01	7.99 ± 4.33	24.61 ± 12.15	0.03 ± 0.00
	Stimulation Pattern 1	3.25 ± 0.75	2.56 ± 1.92	0.03 ± 0.01	10.21 ± 4.86	29.13 ± 15.20	0.03 ± 0.00
	Rest 1	3.08 ± 0.66	2.60 ± 1.99	0.03 ± 0.01	11.16 ± 5.23	15.00 ± 15.00	0.03 ± 0.00
	Stimulation Pattern 2	3.26 ± 0.69	2.73 ± 1.91	0.04 ± 0.01	9.41 ± 3.34	27.88 ± 14.20	0.02 ± 0.00
	Rest 2	3.12 ± 0.72	2.89 ± 2.03	0.02 ± 0.01	8.17 ± 4.21	24.57 ± 14.12	0.03 ± 0.00
DIV8** (n=3)	Basal	2.80 ± 0.25	1.82 ± 0.79	0.11 ± 0.03	19.92 ± 5.11	13.34 ± 3.06	0.04 ± 0.02
	Stimulation Pattern 1	6.84 ± 2.02	9.91 ± 3.50	0.26* ± 0.03	37.63 ± 4.80	83.71* ± 8.31	0.13* ± 0.02
	Rest 1	3.17 ± 0.42	3.41* ± 1.09	0.17 ± 0.02	32.62 ± 5.51	12.91 ± 8.47	0.05 ± 0.03
	Stimulation Pattern 2	5.54 ± 1.19	9.68 ± 3.28	0.15 ± 0.04	33.88 ± 4.64	82.57* ± 8.13	0.13* ± 0.02
	Rest 2	2.07* ± 0.14	0.98 ± 0.49	0.09 ± 0.04	18.23 ± 9.82	7.79 ± 4.59	0.04 ± 0.02
DIV13** (n=4)	Basal	1.67 ± 0.30	0.20 ± 0.11	0.02 ± 0.01	11.34 ± 6.94	2.73 ± 1.73	0.02 ± 0.00
	Stimulation Pattern 1	2.99* ± 0.26	2.27 ± 1.06	0.15* ± 0.04	24.95 ± 11.41	52.83 ± 18.94	0.07 ± 0.02
	Rest 1	1.32 ± 0.36	0.27 ± 0.16	0.05 ± 0.03	10.62 ^a ± 6.22	0	0.01 ± 0.00
	Stimulation Pattern 2	2.16* ^a ± 0.23	1.22 ± 0.53	0.09* ± 0.03	17.16* ± 7.37	36.26 ± 19.88	0.05 ± 0.02
	Rest 2	1.24 ± 0.3775	0.02 ± 0.02	0	7.21 ± 6.68	0	0.01 ± 0.00
DIV17 (n=4)	Basal	9.91 ± 2.63	16.98 ± 5.82	0.16 ± 0.04	31.24 ± 9.74	85.62 ± 18.59	0.12 ± 0.05
	Stimulation Pattern 1	9.61 ^c ± 2.41	16.80 ± 5.50	0.18 ± 0.04	31.95 ± 6.74	69.86 ± 23.93	0.09 ^c ± 0.02
	Rest 1	8.77 ± 2.78	15.46 ^b ± 5.63	0.11 ± 0.05	17.97 ^b ± 4.92	81.81 ± 24.04	0.06 ± 0.01
	Stimulation Pattern 2	9.40 ^c ± 2.39	16.75 ± 5.62	0.18 ± 0.04	36.83 ± 11.55	56.68 ± 26.78	0.11 ± 0.04

	Rest 2	9.51 ± 2.90	15.95 ± 5.80	0.15 ± 0.06	27.93 ± 9.51	53.83 ± 28.65	0.10 ± 0.05
--	--------	-------------	--------------	-------------	--------------	---------------	-------------

Values are displayed as weighted averages ± SEM

*** (Rest 1 for DIV8 and 13 was reduced to 50 sec post-hoc due to human error. Stimulation pattern 1 lasted longer than the intended 60 sec)*

** Significant change ($p < 0.05$)*

^a Significant difference in percent change between DIV13 and DIV8 ($p < 0.05$)

^b Significant difference in percent change between DIV17 and DIV13 ($p < 0.05$)

^c Significant difference in percent change between DIV17 and DIV8 ($p < 0.05$)

7. CONCLUDING REMARKS AND FUTURE DIRECTIONS

In this study we proved that neural networks derived from the HBG3 ChR2 mESC demonstrate functional optical control with blue LED light exposure. These networks also displayed evidence of functional neurotransmitter receptors by their electrophysiological responses to pharmacological treatments. However, this was a preliminary study to establish basic functionality of this cell line. There are countless experiments to further substantiate the model uses for this cell line. In this section, I will discuss some of those possibilities.

This experiment adopted a basic pharmacological protocol to justify a degree of functionality of several essential neurotransmitter receptors. To affirm a greater degree of functionality, the use of scaled concentrations of the pharmacological treatments would supply response curve information. This is an important step for future work after seeing such stark responses from the concentrations used for GABA (100 μ M) and AMPA (5 μ M) and the inability to perform substantial analysis from the treated data. Lower

concentrations of GABA (20 μ M) have shown to have significant inhibitor effects on cultured rat motor neurons but supplied enough data for bursting analysis [59]. As a mixed neural culture, toxicity levels for compounds are not well established. There is evidence that NMDA concentrations greater than 40 μ M elicit excitotoxic effects in cultured rat spinal neurons on the MEA [24]. Considering that the differentiation protocol used in this study drives spinal fate differentiation through Shh and RA pathway stimulation in order to get motor neurons, comparing pharmacological response curves to that of primary cultures would be beneficial. This study only established functionality for GABA and Glutamate receptors, with the presence of motor neurons, nicotinic compounds such as acetylcholine or atropine to test the nicotinic or muscarinic receptors would validate a wider variety of receptor functionality for more comprehensive analysis. The electrophysiological effects from treatments of biogenic amines, such as serotonin and dopamine would provide interesting and valuable information for establishing a model for more complex neurological functions. Biogenic amine analysis would also demonstrate the potential for disease models whose phenotypes are characterized by malfunctions in serotonergic or dopaminergic neurons or cell death, such as Parkinson's [60].

Future experiments would also benefit from taking advantage of the optical functionality of these cells. Optogenetics provides the advantages over pharmacological and electrical stimulation with the ability for controlled temporal and spatial stimulation that doesn't harm the physiology of the cell [58]. Using channelrhodopsin-2 (ChR2) active networks, researchers have successfully demonstrated neural network using primary hippocampal cultures on the MEA. Repeated light stimulation at 40Hz for 10 minutes resulted in networks maintaining an increased mean firing rate (MFR) from pre-stimulation recordings 70 minutes post stimulation [11]. Specific light stimulation protocols have also demonstrated to increase interneuronal synchronization on neural networks from isolated hippocampal neurons [58]. Comparing this cell line's network plasticity and bursting pattern responses to primary cultures could eventually allow for modeling diseases with characterized burst patterns, such as Epilepsy.

Optogenetics can easily be combined with pharmacology studies. Using blockers to inhibit specific neurotransmitter responses, researchers can identify which neurotransmitter receptors are responsible for the optically stimulated response. By using a mix of 2-amino-5-phosphonopentanoic acid (APV) and Picrotoxin to block NMDA activity, or 2,3-Dioxo-6-nitro-1,2,3,4-

tetrahydrobenzo[f]quinoxaline-7-sulfonamide (NBQX) and Picrotoxin to inhibit AMPA activity, it was established that both glutamate receptors contribute to optically augmented network synchrony [58].

ChR2 was transfected into these cells onto the Rosa26 locus via nucleofection. This locus is present in all cell types and protected from gene-silencing effects [61], meaning that ChR2 is constitutively expressed or “always on.” Due to this cell line’s integration of GFP into motor-neuron specific HB9 promoter gene, motor neurons can be isolated through Fluorescence Activated Cell Sorting (FACS). With proper optical stimulation technology and utilizing microfluidics, pure cell populations allow for interesting potential on the MEA utilizing both ChR2 positive and ChR2 negative cells. Microfluidic technology uses microscopic devices that can be designed to possess physical barriers with the ability to isolate cells or cell populations [62]. Microfluidic designs have demonstrated the capability of isolating neural populations, but allowing axons to growth and pass through the barrier[63]. Possible informative set ups on the MEA include separate channels for ChR2 positive motor neurons and ChR2 negative C2C12 muscle cells to analyze the electrophysiological response of the muscle cells to light activated motor neurons. Although ChR2 positive stem cell derived motor

neurons transplanted into denervated mice have successfully shown the ability for optical stimulation of the native muscle [49], the described MEA protocol provides alternative advantages. Combined optical stimulation and MEA technology allows for simple set up of controls with the ability to alter light intensity, pulse width, and pulse frequency to observe the effects and efficiency on muscle response. Another set up that benefits from microfluidic technology would be ChR2 positive interneurons with ChR2 negative motor neurons. The communication between interneurons and motor neurons is an essential part of the motor pathway, but is poorly understood and this set up could provide constructive information for a sharpened grasp of their relationship. Microfluidic design is up to the creator allowing for set ups such as ChR2 positive interneurons, ChR2 negative motor neurons, and ChR2 negative skeletal muscle cells, potentially creating the possibility for countless cell-communication combinations.

There is still much we do not fully understand about neurological functions. Due to these limitations, many neurological disorders and diseases exist without preventative measures or treatments. Combining stem cell technology with both optogenetics and MEA technology opens up the

possibilities for limitless studies to analyze neural network electrophysiology and functions with the hope of one day finding cures to all that ails us.

REFERENCES

1. KEELE, S.W., *MOVEMENT CONTROL IN SKILLED MOTOR PERFORMANCE*1. Psychological Bulletin, 1968. **70**(6 PART 1).
2. Synofzik, M., G. Vosgerau, and A. Newen, *I move, therefore I am: a new theoretical framework to investigate agency and ownership*. Conscious Cogn, 2008. **17**(2): p. 411-24.
3. Gandevia, S.C., *Roles for perceived voluntary motor commands in motor control*. Trends in Neurosciences, 1987. **10**(2): p. 81-85.
4. Scott, S.H., *Optimal feedback control and the neural basis of volitional motor control*. Nature Reviews Neuroscience, 2004. **5**(7): p. 532-546.
5. Winter, D.A., *Biomechanics and Motor Control of Human Movement*. 2009: John Wiley & Sons. 386.
6. Goulding, M., *Circuits controlling vertebrate locomotion: moving in a new direction*. Nat Rev Neurosci, 2009. **10**(7): p. 507-18.
7. Jessell, T.M., *Neuronal specification in the spinal cord: inductive signals and transcriptional codes*. Nat Rev Genet, 2000. **1**(1): p. 20-9.
8. Wichterle, H., et al., *Directed differentiation of embryonic stem cells into motor neurons*. Cell, 2002. **110**(3): p. 385-97.
9. Byrne, J.H. *Neuroscience Online*. Introduction to Neurons and Neuronal Networks 2014 [cited 2014 September 16th]; Available from: <http://neuroscience.uth.tmc.edu/s1/introduction.html>.
10. Takazawa, T., et al., *Maturation of Spinal Motor Neurons Derived from Human Embryonic Stem Cells*. PLoS ONE, 2012. **7**(7): p. e40154.
11. Lignani, G., et al., *Long-term optical stimulation of channelrhodopsin-expressing neurons to study network plasticity*. Front Mol Neurosci, 2013. **6**: p. 22.

12. Huttenlocher, P.R., *NEURAL PLASTICITY*. 2009: Harvard University Press. 285.
13. *Neuropsychopharmacology: The Fifth Generation of Progress*. Vol. 5. 2002, Philadelphia, Pennsylvania: Lippincott, Williams, & Wilkins, .
14. *Axion Biosystems. Microelectrode Arrays 2012* [cited 2014 September 19th]; Available from: <http://www.axionbiosystems.com/>.
15. Gross, G.W., A.N. Williams, and J.H. Lucas, *Recording of spontaneous activity with photoetched microelectrode surfaces from mouse spinal neurons in culture*. *J Neurosci Methods*, 1982. **5**(1-2): p. 13-22.
16. Spira, M.E. and A. Hai, *Multi-electrode array technologies for neuroscience and cardiology*. *Nat Nanotechnol*, 2013. **8**(2): p. 83-94.
17. Thomas, C.A., Jr., et al., *A miniature microelectrode array to monitor the bioelectric activity of cultured cells*. *Exp Cell Res*, 1972. **74**(1): p. 61-6.
18. Buzanska, L., et al., *Neural stem cells from human cord blood on bioengineered surfaces--novel approach to multiparameter bio-tests*. *Toxicology*, 2010. **270**(1): p. 35-42.
19. Robinette, B.L., et al., *In vitro assessment of developmental neurotoxicity: use of microelectrode arrays to measure functional changes in neuronal network ontogeny*. *Front Neuroeng*, 2011. **4**: p. 1.
20. Ban, J., et al., *Embryonic stem cell-derived neurons form functional networks in vitro*. *Stem Cells*, 2007. **25**(3): p. 738-49.
21. Chiappalone, M., et al., *Burst detection algorithms for the analysis of spatio-temporal patterns in cortical networks of neurons*. *Neurocomputing*, 2005. **65-66**(0): p. 653-662.
22. Bakkum, D.J., et al., *Parameters for burst detection*. *Frontiers in Computational Neuroscience*, 2013. **7**: p. 193.
23. Kapucu, F.E., et al., *Burst analysis tool for developing neuronal networks exhibiting highly varying action potential dynamics*. *Frontiers in Computational Neuroscience*, 2012. **6**: p. 38.
24. Johnstone, A.F., et al., *Microelectrode arrays: a physiologically based neurotoxicity testing platform for the 21st century*. *Neurotoxicology*, 2010. **31**(4): p. 331-50.

25. González-Montoro, A., et al., *Bootstrap testing for cross-correlation under low firing activity*. Journal of Computational Neuroscience, 2015: p. 1-11.
26. McConnell, E.R., et al., *Evaluation of multi-well microelectrode arrays for neurotoxicity screening using a chemical training set*. Neurotoxicology, 2012. **33**(5): p. 1048-57.
27. Valdivia, P., et al., *Multi-well microelectrode array recordings detect neuroactivity of ToxCast compounds*. Neurotoxicology, 2014. **44**: p. 204-17.
28. Cooper, J.R. and R.H. Roth, *The biochemical basis of neuropharmacology*. 2003: Oxford University Press.
29. Reiner, A., J. Levitz, and E.Y. Isacoff, *Controlling ionotropic and metabotropic glutamate receptors with light: principles and potential*. Current Opinion in Pharmacology, 2015. **20**(0): p. 135-143.
30. Barbon, A. and S. Barlati, *Glutamate receptor RNA editing in health and disease*. Biochemistry (Moscow), 2011. **76**(8): p. 882-889.
31. Hanada, T., *The discovery and development of perampanel for the treatment of epilepsy*. Expert Opinion on Drug Discovery, 2014. **9**(4): p. 449-458.
32. Burnashev, N. and P. Szepietowski, *NMDA receptor subunit mutations in neurodevelopmental disorders*. Current Opinion in Pharmacology, 2015. **20**(0): p. 73-82.
33. Illes, S., et al., *Development and pharmacological modulation of embryonic stem cell-derived neuronal network activity*. Exp Neurol, 2007. **207**(1): p. 171-6.
34. Heikkila, T.J., et al., *Human embryonic stem cell-derived neuronal cells form spontaneously active neuronal networks in vitro*. Exp Neurol, 2009. **218**(1): p. 109-16.
35. Bormann, J., *The 'ABC' of GABA receptors*. Trends in Pharmacological Sciences, 2000. **21**(1): p. 16-19.
36. Chabrol, F.P., S.J. Eglén, and E. Sernagor, *GABAergic control of retinal ganglion cell dendritic development*. Neuroscience, 2012. **227**(0): p. 30-43.
37. Klomjai, W., et al., *Changes in spinal inhibitory networks induced by furosemide in humans*. The Journal of Physiology, 2014. **592**(13): p. 2865-2879.

38. Zeilhofer, H.U., W.T. Ralvenius, and M.A. Acuña, *Chapter Four - Restoring the Spinal Pain Gate: GABAA Receptors as Targets for Novel Analgesics*, in *Advances in Pharmacology*, R. Uwe, Editor. 2015, Academic Press. p. 71-96.
39. Behrens, C.J., L.P. Van Den Boom, and U. Heinemann, *Effects of the GABAA receptor antagonists bicuculline and gabazine on stimulus-induced sharp wave-ripple complexes in adult rat hippocampus in vitro*. *European Journal of Neuroscience*, 2007. **25**(7): p. 2170-2181.
40. Vandenberg, R.J., et al., *Glycine transport inhibitors for the treatment of pain*. *Trends in Pharmacological Sciences*, 2014. **35**(8): p. 423-430.
41. Zafra, F., et al., *Glycine transporters are differentially expressed among CNS cells*. *J Neurosci*, 1995. **15**(5 Pt 2): p. 3952-69.
42. Kistemaker, L.E.M. and R. Gosens, *Acetylcholine beyond bronchoconstriction: roles in inflammation and remodeling*. *Trends in Pharmacological Sciences*, 2014(0).
43. Paoletti, P., C. Bellone, and Q. Zhou, *NMDA receptor subunit diversity: impact on receptor properties, synaptic plasticity and disease*. *Nat Rev Neurosci*, 2013. **14**(6): p. 383-400.
44. Oda, A. and H. Tanaka, *Activities of nicotinic acetylcholine receptors modulate neurotransmission and synaptic architecture*. *Neural Regeneration Research*, 2014. **9**(24): p. 2128-2131.
45. Li, X.J., et al., *Directed differentiation of ventral spinal progenitors and motor neurons from human embryonic stem cells by small molecules*. *Stem Cells*, 2008. **26**(4): p. 886-93.
46. Meregalli, M., A. Farini, and Y. Torrente, *Stem Cell Therapy for Neuromuscular Diseases*. *Stem Cells in Clinic and Research*. 2011.
47. Arbab, M., S. Baars, and N. Geijsen, *Modeling motor neuron disease: the matter of time*. *Trends Neurosci*, 2014.
48. McCreedy, D.A., et al., *A new method for generating high purity motoneurons from mouse embryonic stem cells*. *Biotechnol Bioeng*, 2014. **111**(10): p. 2041-55.
49. Bryson, J.B., et al., *Optical control of muscle function by transplantation of stem cell-derived motor neurons in mice*. *Science*, 2014. **344**(6179): p. 94-7.

50. Kamm, R.D. and R. Bashir, *Creating living cellular machines*. Ann Biomed Eng, 2014. **42**(2): p. 445-59.
51. Yawo, H., et al., *Optogenetic manipulation of neural and non-neural functions*. Dev Growth Differ, 2013. **55**(4): p. 474-90.
52. Zhang, F., et al., *Circuit-breakers: optical technologies for probing neural signals and systems*. Nat Rev Neurosci, 2007. **8**(8): p. 577-581.
53. Sparta, D.R., et al., *Optogenetic strategies to investigate neural circuitry engaged by stress*. Behav Brain Res, 2013. **255**: p. 19-25.
54. Caggiano, V., M. Sur, and E. Bizzi, *Rostro-caudal inhibition of hindlimb movements in the spinal cord of mice*. PLoS One, 2014. **9**(6): p. e100865.
55. Wagenaar, D.A. and S.M. Potter, *Real-time multi-channel stimulus artifact suppression by local curve fitting*. Journal of Neuroscience Methods, 2002. **120**(2): p. 113-120.
56. Molnár, E., *Long-term potentiation in cultured hippocampal neurons*. Seminars in Cell & Developmental Biology, 2011. **22**(5): p. 506-513.
57. Heimer, G., et al., *Synchronizing activity of basal ganglia and pathophysiology of Parkinson's disease*, in *Parkinson's Disease and Related Disorders*. 2006, Springer. p. 17-20.
58. El Hady, A., et al., *Optogenetic stimulation effectively enhances intrinsically generated network synchrony*. Frontiers in Neural Circuits, 2013. **7**: p. 167.
59. Zhang, H.M., et al., *Neuronal and network activity in networks of cultured spinal motor neurons*. Neuroreport, 2009. **20**(9): p. 849-54.
60. Kong, P., et al., *Neuroprotection of MAO-B inhibitor and dopamine agonist in Parkinson disease*. Int J Clin Exp Med, 2015. **8**(1): p. 431-9.
61. Irion, S., et al., *Identification and targeting of the ROSA26 locus in human embryonic stem cells*. Nat Biotech, 2007. **25**(12): p. 1477-1482.
62. Inglis, D., *Microfluidic devices for cell separation*. 2007: Princeton University.
63. Jang, J.M., et al., *Engineering controllable architecture in matrigel for 3D cell alignment*. ACS Appl Mater Interfaces, 2015. **7**(4): p. 2183-8.